AFM: some measurements

Formation and evolution of self-organized Au nanorings on indium-tin-oxide surface

F. Ruffino,[1,2,a)] I. Crupi,[2] F. Simone,[1,2] and M. G. Grimaldi[1,2]
[1]*Dipartimento di Fisica e Astronomia, Università di Catania, via S. Sofia 64, 95123 Catania, Italy*
[2]*MATIS CNR-IMM, via S. Sofia 64, 95123 Catania, Italy*

(Received 20 October 2010; accepted 18 December 2010; published online 10 January 2011)

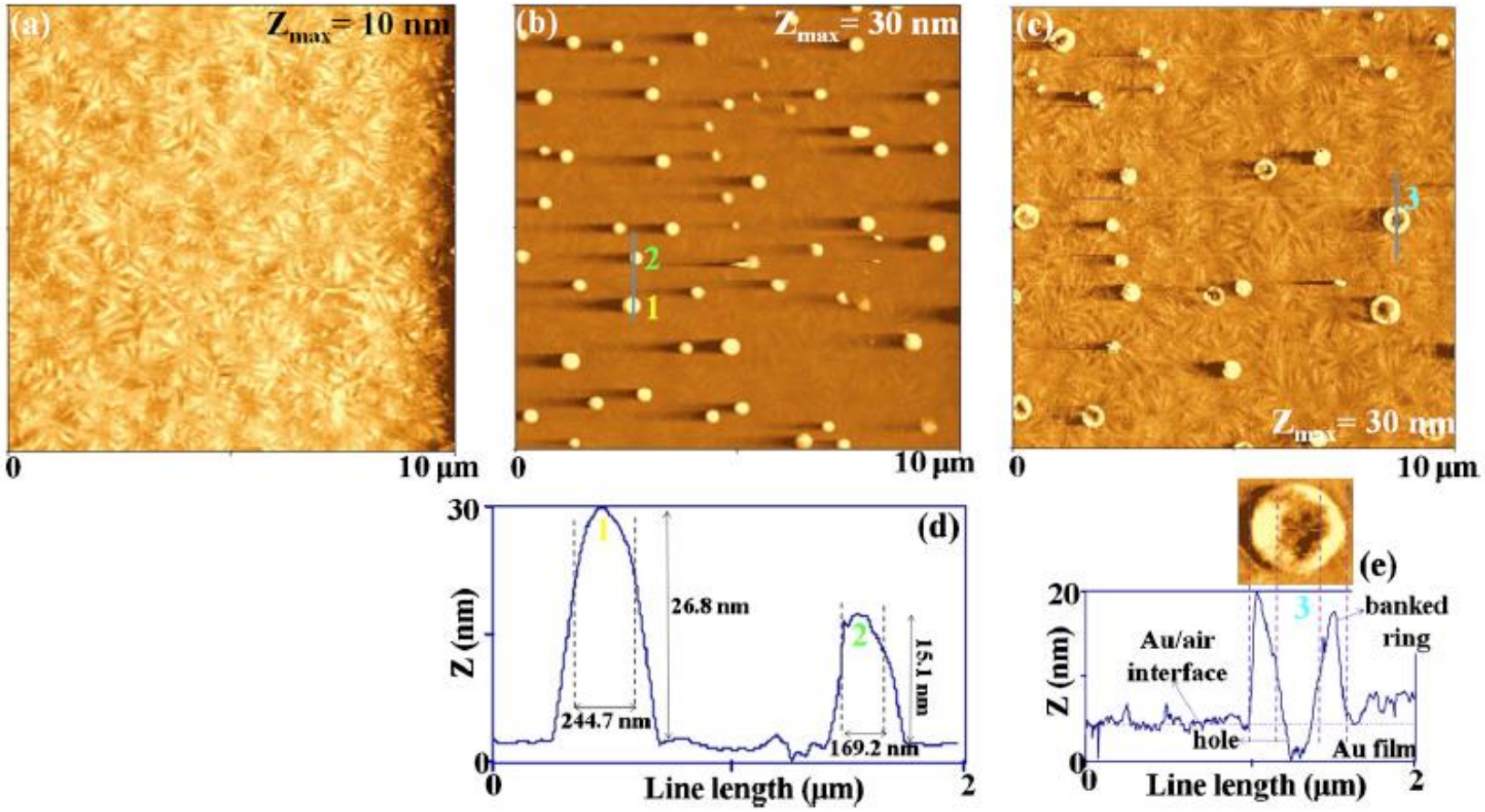

FIG. 1. (Color online) 10 μm $\times$10 μm AFM image of (a) the starting ITO surface, (b) 25 nm of Au sputter-deposited on the ITO surface, (c) 25 nm of Au sputter-deposited on the ITO surface annealed at 573 K-3600 s. (d) Cross-sectional AFM line-scanning profile of three NCs labeled as 1, and 2 in (b). (e) Cross-sectional AFM line-scanning profile of the NR labeled as 3 in (c).

Ruffino *et al. Nanoscale Research Letters* 2011, **6**:112
http://www.nanoscalereslett.com/content/6/1/112

Nanoscale Research Letters
a SpringerOpen Journal

NANO EXPRESS Open Access

Atomic force microscopy investigation of the kinetic growth mechanisms of sputtered nanostructured Au film on mica: towards a nanoscale morphology control

Francesco Ruffino[1,2], Vanna Torrisi[3*], Giovanni Marletta[3], Maria Grazia Grimaldi[1,2]

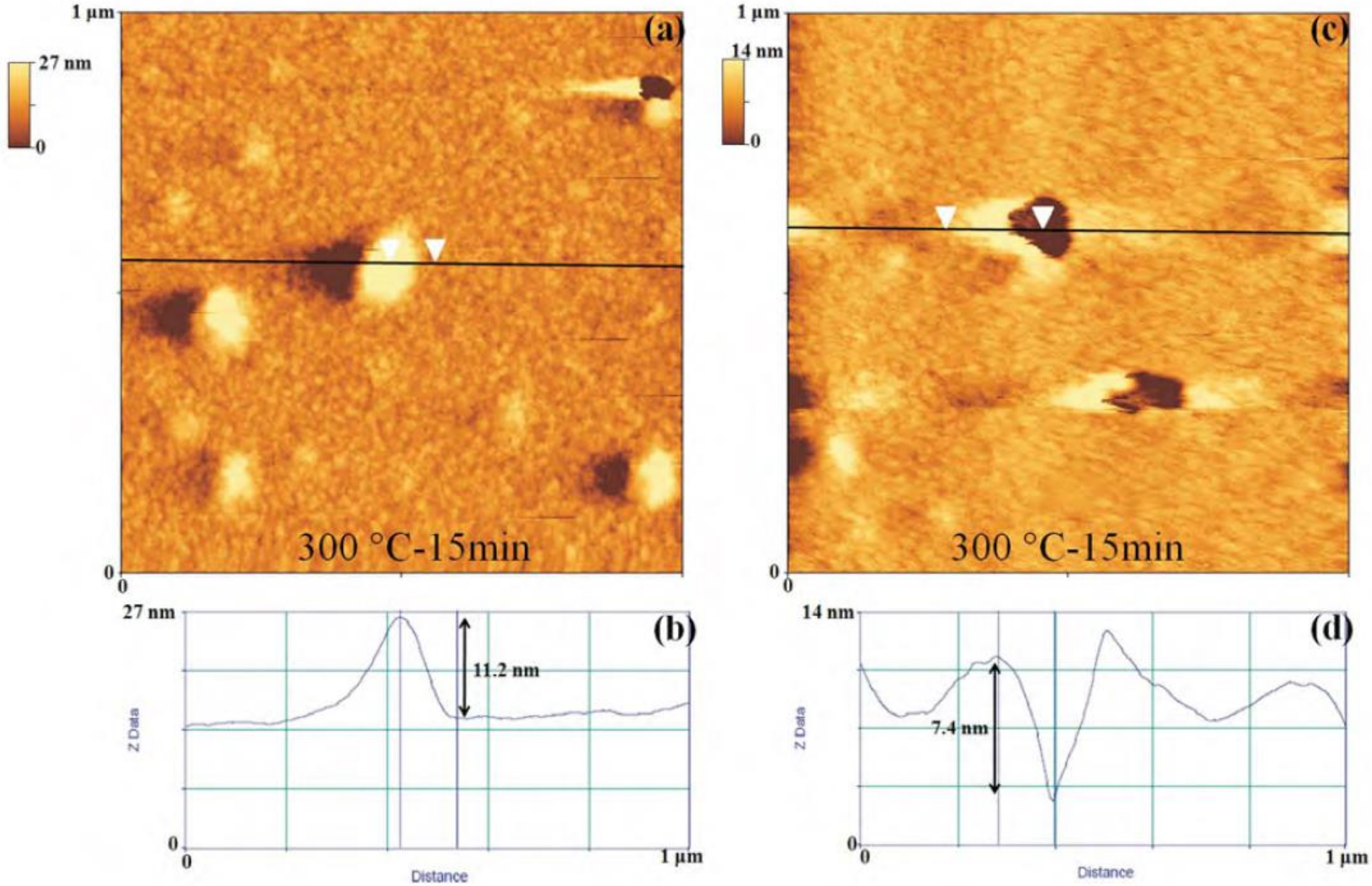

Figure 4 AFM images and section masurements of the thermally processed Au film: (a, c) 1 µm × 1 µm AFM scans of the Au film thermally processed at 573 K-15 min; (b) section measurement to estimate the height (11.2 nm) of a nucleated Au cluster; (d) section measurement to estimate the depth (7.4 nm) of a hole in the Au film.

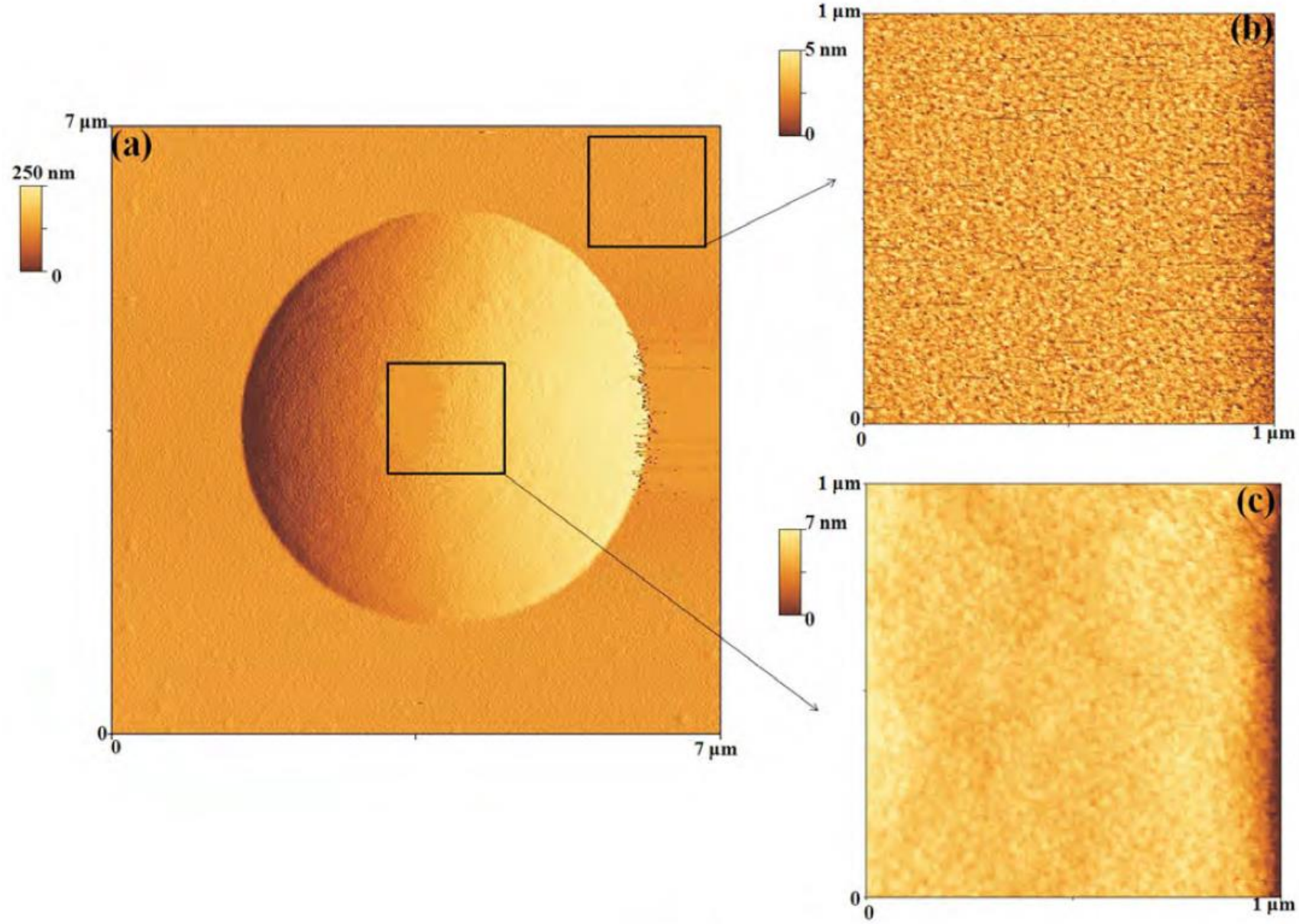

Figure 6 AFM image of a single Au cluster: (a) 7 µm × 7 µm AFM scan of the Au film thermally processed at 773 K-60 min, focusing, in particular, on an Au cluster; (b) 1 µm × 1 µm AFM scan of the underlaying Au film; (c) 1 µm × 1 µm AFM scan on the Au cluster, evidencing its granular structure.

Torrisi *et al. Nanoscale Research Letters* 2011, **6**:167
http://www.nanoscalereslett.com/content/6/1/167

Nanoscale Research Letters
a SpringerOpen Journal

NANO EXPRESS Open Access

Memory effects in annealed hybrid gold nanoparticles/block copolymer bilayers

Vanna Torrisi[1*], Francesco Ruffino[2], Antonino Licciardello[1], Maria Grazia Grimaldi[2], Giovanni Marletta[1]

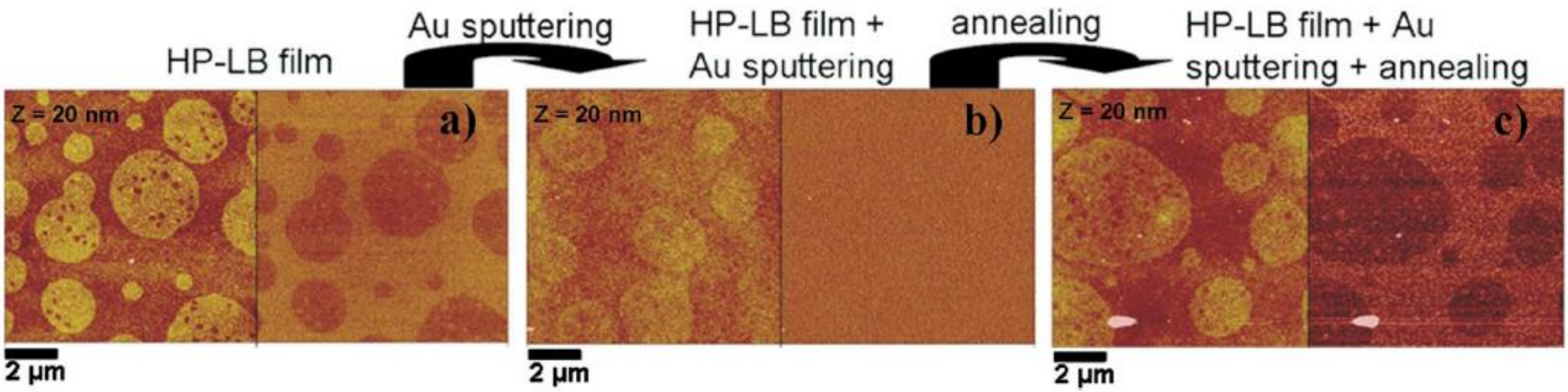

Figure 2 AFM images of the three steps of sample preparation: **(a)** HP-LB film of P*n*BuA-*b*-PAA; **(b)** HP-LB film covered with Au nanoparticles deposited by sputtering; **(c)** annealed bilayer (115°C, 15 min).

AMERICAN SCIENTIFIC PUBLISHERS

Science of Advanced Materials
Vol. 4, pp. 708–718, 2012
(www.aspbs.com/sam)

Formation and Evolution of Nanoscale Metal Structures on ITO Surface by Nanosecond Laser Irradiations of Thin Au and Ag Films

F. Ruffino[1,2,*], E. Carria[1,2], S. Kimiagar[1,3], I. Crupi[2], F. Simone[1,2], and M. G. Grimaldi[1,2]

[1]*Dipartimento di Fisica ed Astronomia-Università di Catania, via S. Sofia 64, 95123 Catania, Italy*
[2]*MATIS IMM-CNR, via S. Sofia 64, 95123 Catania, Italy*
[3]*Islamic Azad University, Central Tehran Branch, Tehran, Iran*

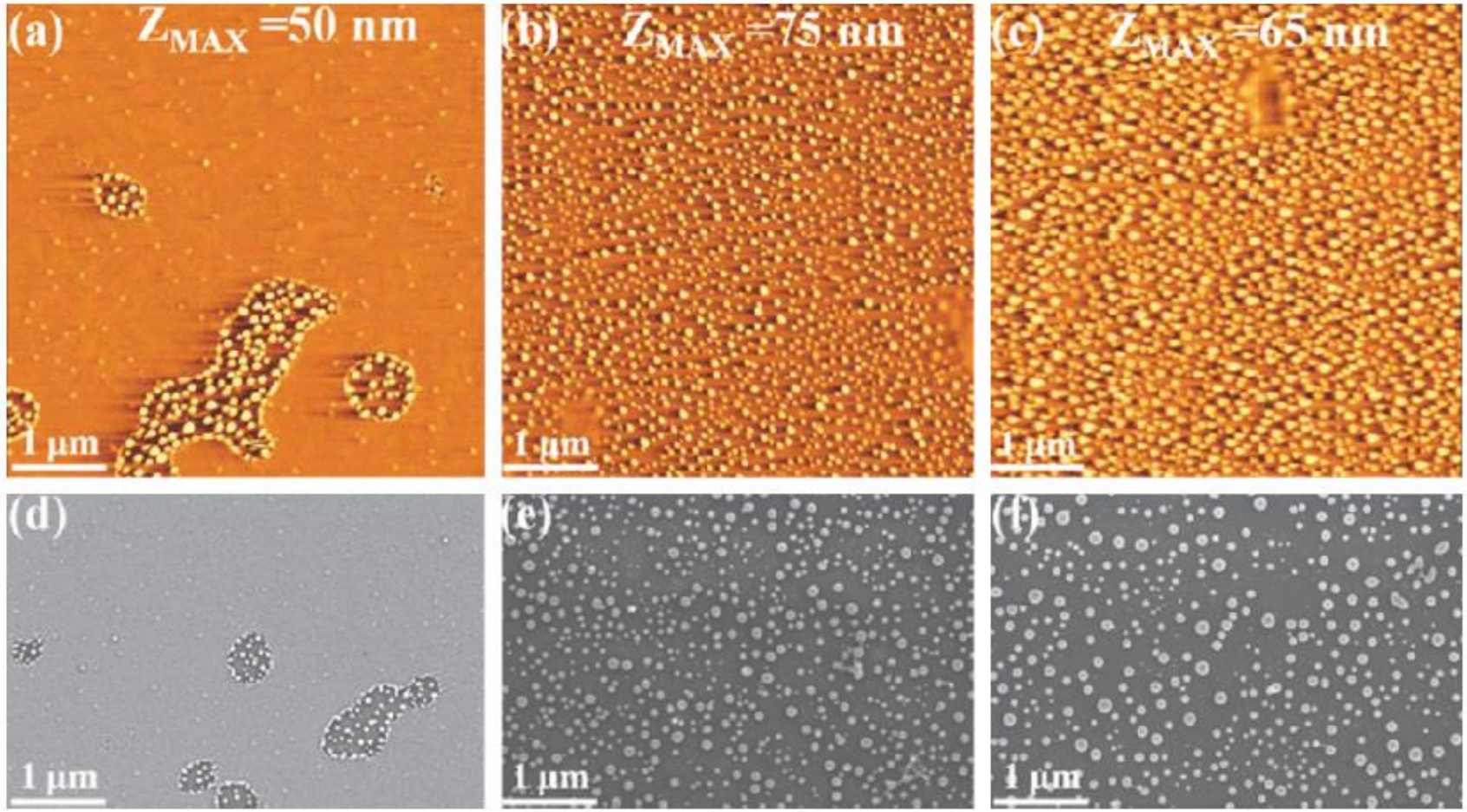

Fig. 2. AFM ((a)–(c)) and SEM ((d)–(f)) images of the 5 nm thick Au film on ITO irradiated by 500 mJ/cm^2 ((a) and (d)), 750 mJ/cm^2 ((b) and (e)), 1000 mJ/cm^2 ((c) and (f)).

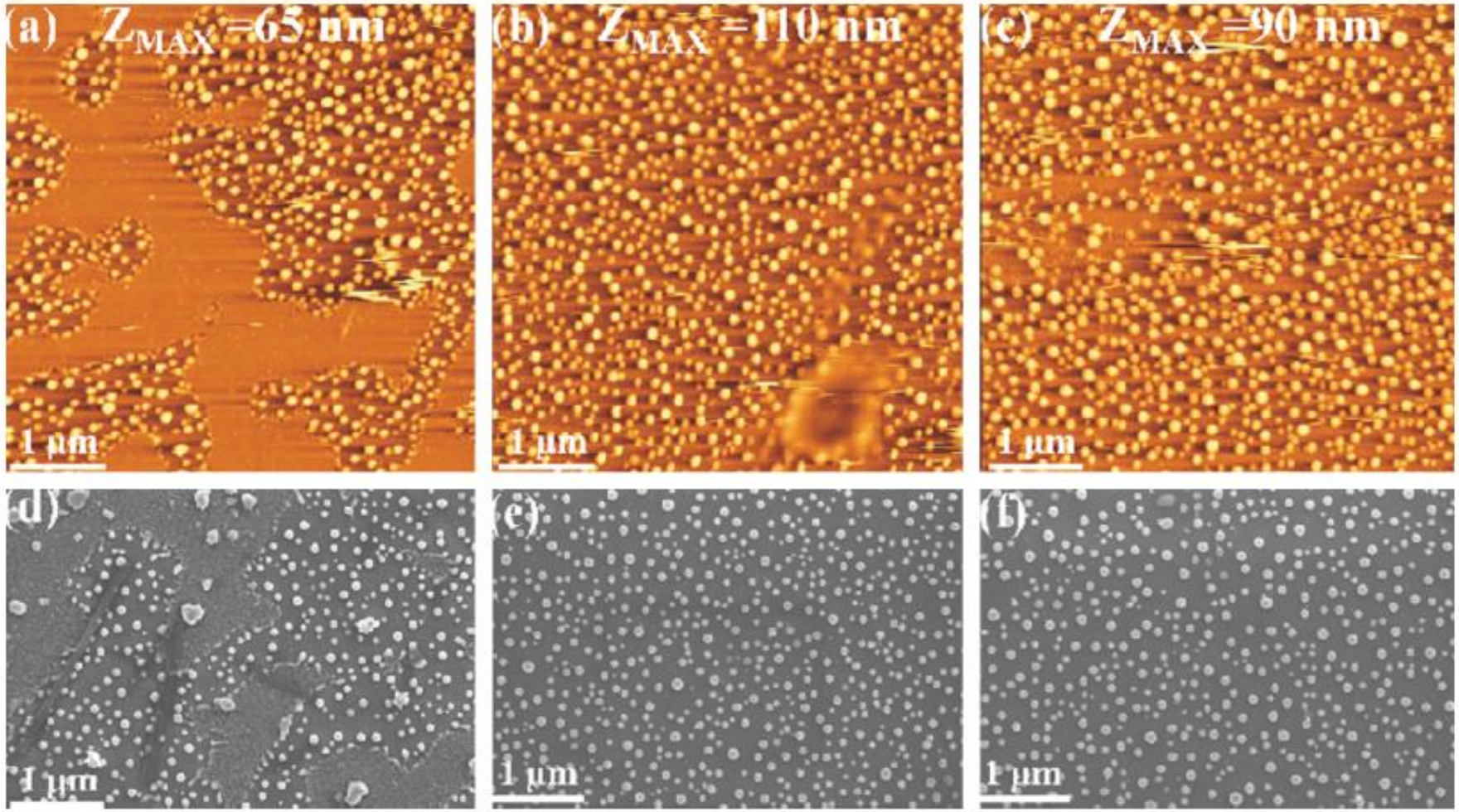

Fig. 3. AFM ((a)–(c)) and SEM ((d)–(f)) images of the 5 nm thick Ag film on ITO irradiated by 500 mJ/cm^2 ((a) and (d)), 750 mJ/cm^2 ((b) and (e)), 1000 mJ/cm^2 ((c) and (f)).

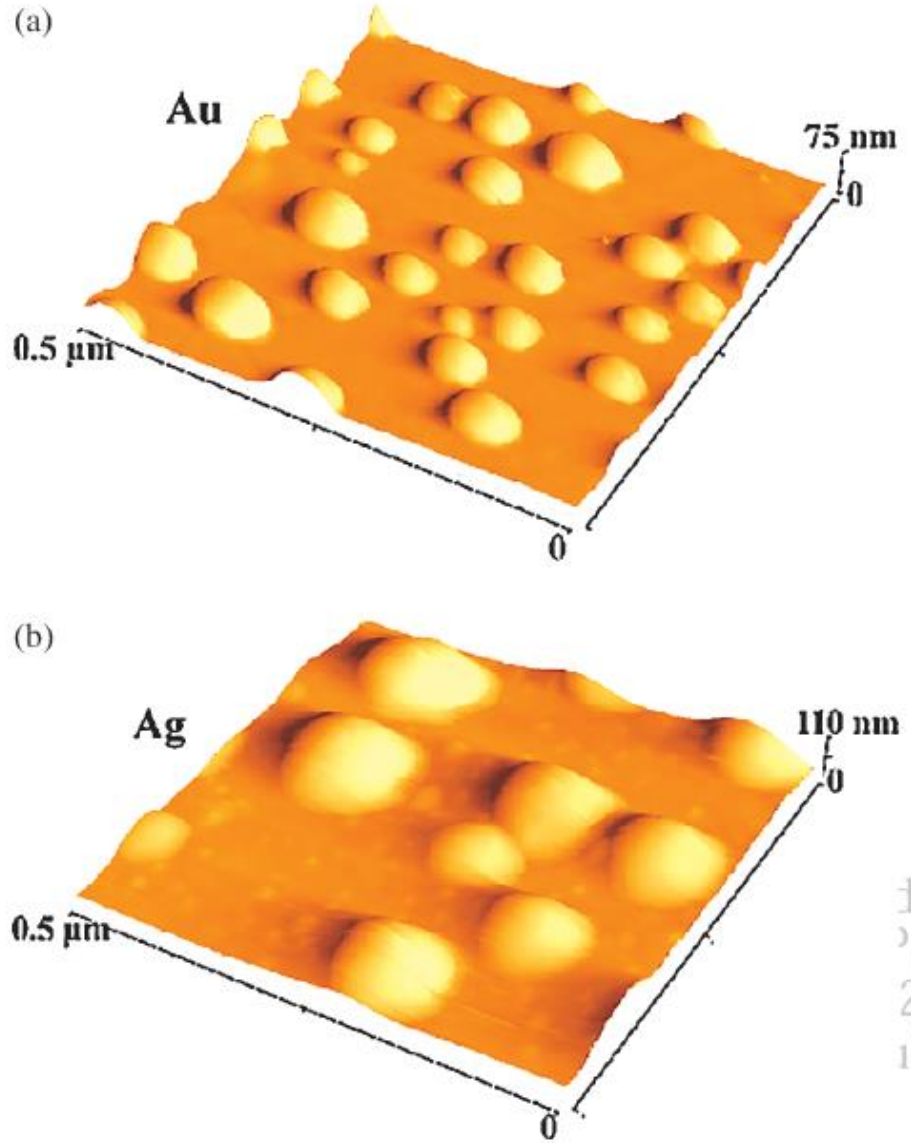

Fig. 4. Three-dimensional reconstructions of 0.5 μm $\times$ 0.5 μm AFM images the (a) Au and (b) Ag films irradiated by 750 mJ/cm^2.

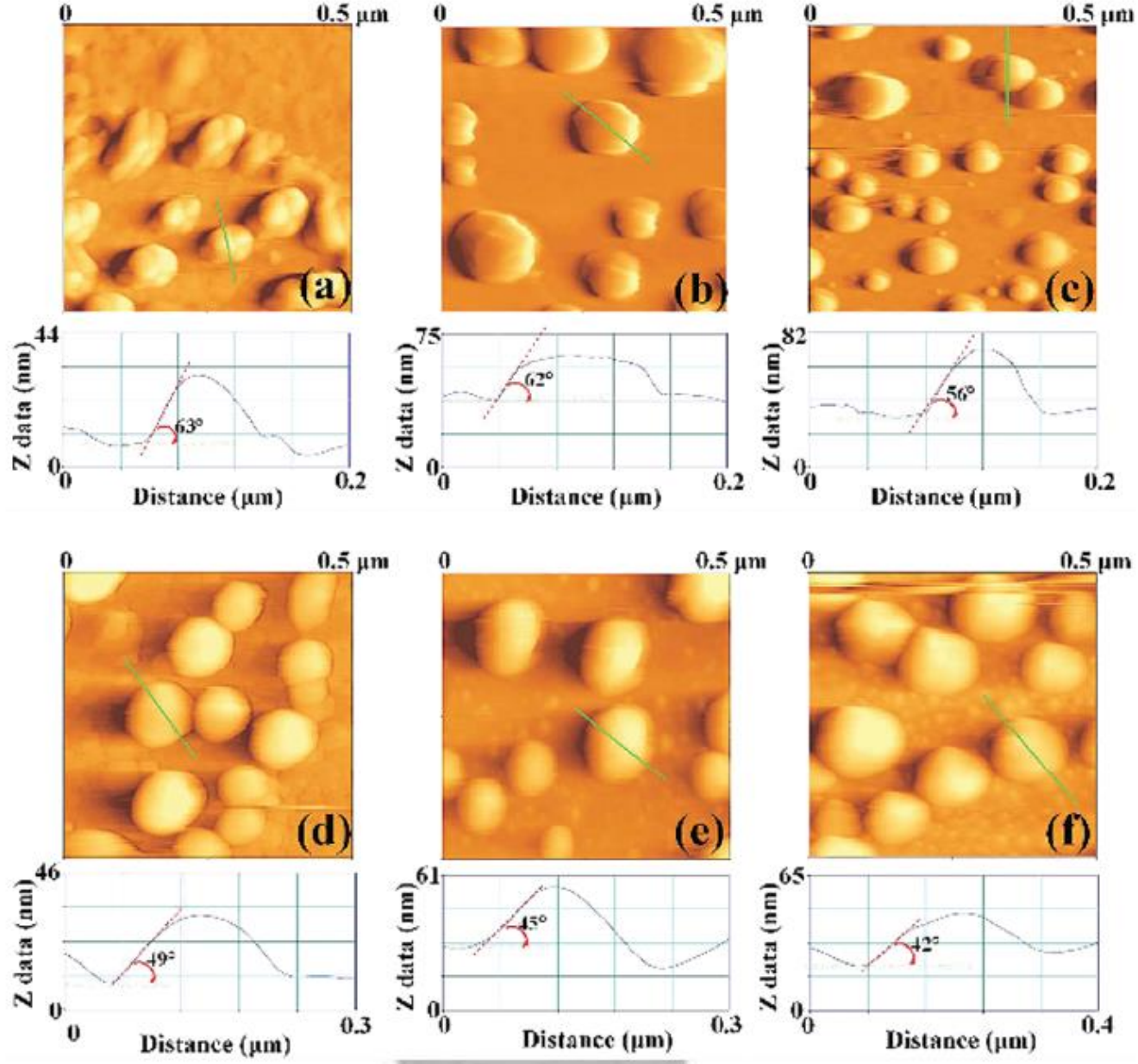

Fig. 8. 0.5 μm $\times$ 0.5 μm AFM images of the samples and line profile sections of representative isolate NCs for the contact angle measurements: (a)–(c) Au film irradiated by 500 (a), 750 (b), and 1000 mJ/cm^2 (c); (d)–(f) Ag film irradiated by 500 (d), 750 (e), and 1000 mJ/cm^2 (f).

Structural and optical properties of highly Er-doped Yb-Y disilicate thin films

Paolo Cardile,[1] Maria Miritello,[1,*] Francesco Ruffino,[1,2] and Francesco Priolo[1,2]

[1]CNR-IMM MATIS, via S. Sofia 64, I-95123 Catania, Italy
[2]Dipartimento di Fisica e Astronomia, Università di Catania, via S. Sofia 64, I-95123 Catania, Italy

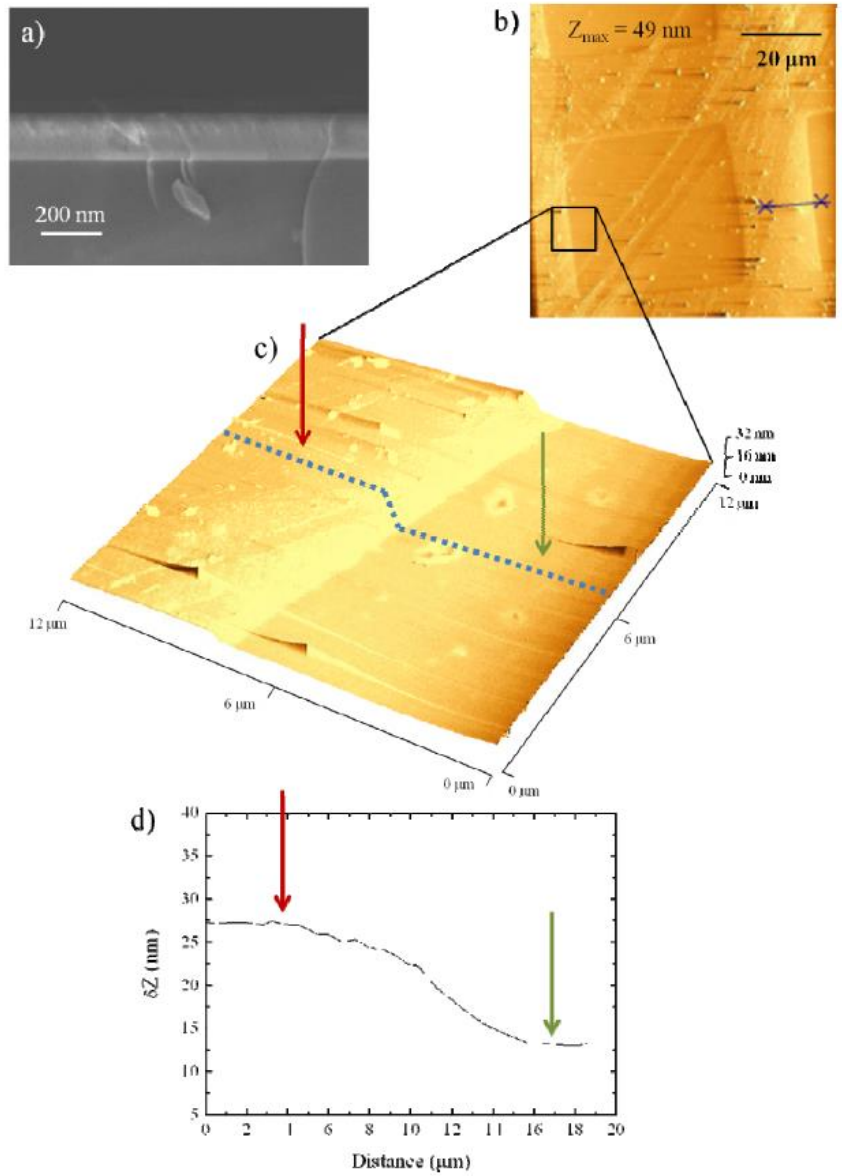

Fig. 2. (a) Cross sectional SEM image of an as deposited Yb-Y disilicate. (b) AFM measurements on an as-implanted sample, after removing a masking grating. (c) AFM zoom-in reporting the step height in a 3D picture. (d) Analytical measurement of the step height.

Fig. 2 **a** Scheme of the normal deposition ($\alpha = 0°$) configuration and of the expected pattern of the Au and Ag films (cross-section view). **b** Scheme of the oblique deposition ($\alpha = 42°$) configuration and of the expected pattern of the Au and Ag films (cross-section view)

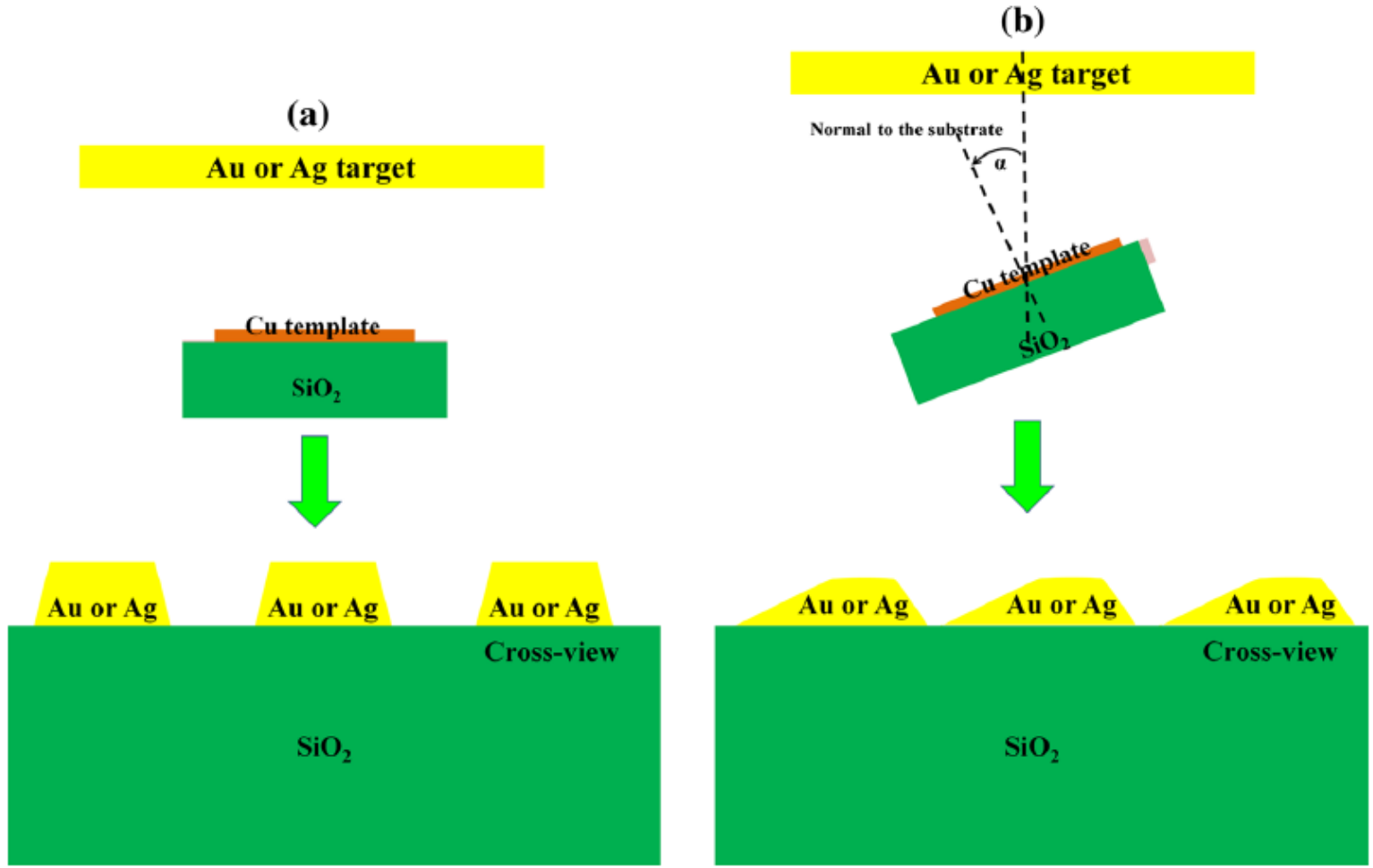

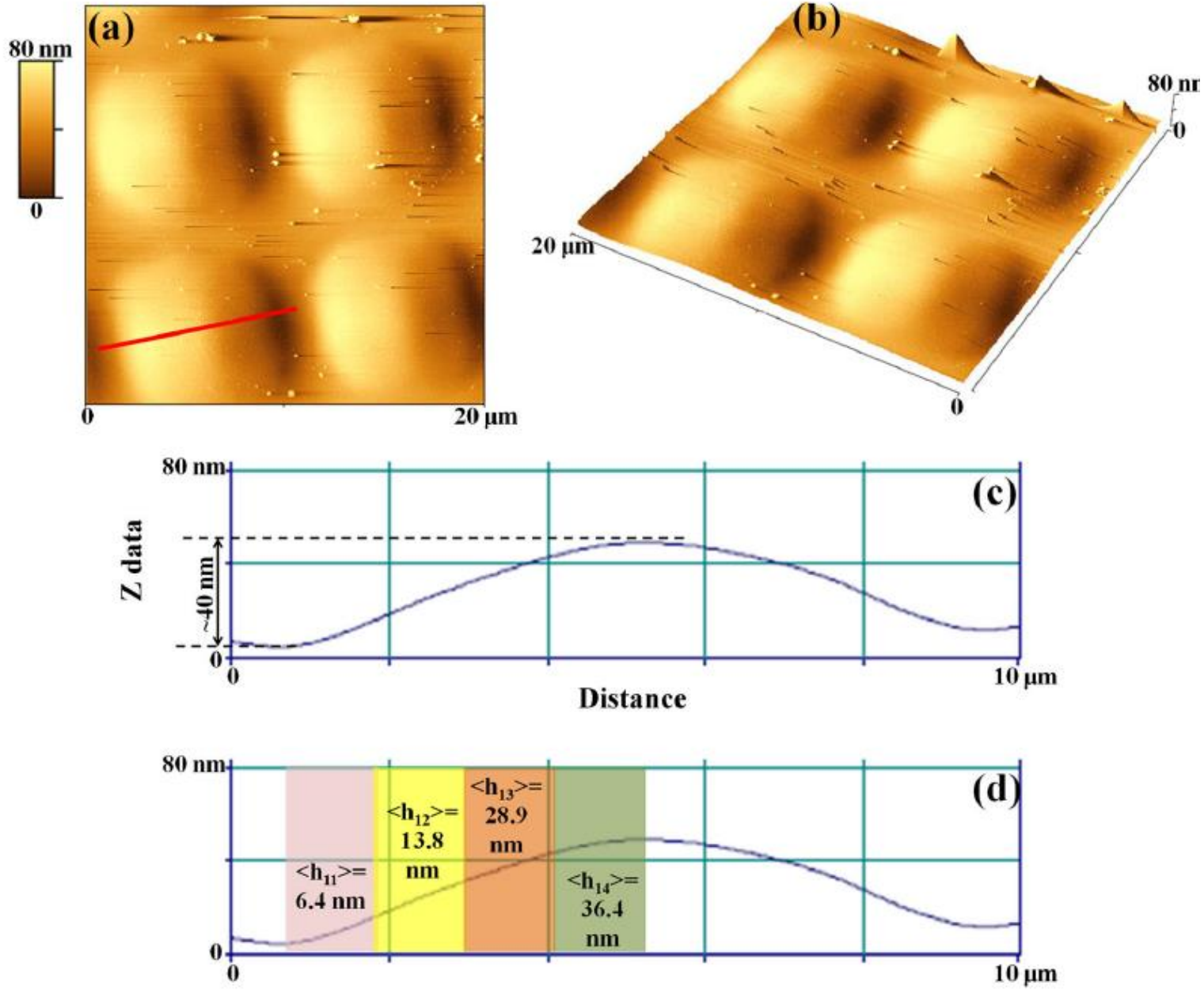

Fig. 3 **a** Two-dimensional AFM scan (20 µm × 20 µm) of the 40 nm-thick Au film deposited through the lithographic mask in normal condition ($\alpha = 0°$). **b** Three-dimensional reconstruction of the AFM image in (**a**). **c** Cross-line profile of a Au square corresponding to the *red line* in (**a**). From this symmetric cross-line profile, from the center to the edge the square is divided in four regions assigning to each region an effective height $\langle h_{ij} \rangle$ (**d**)

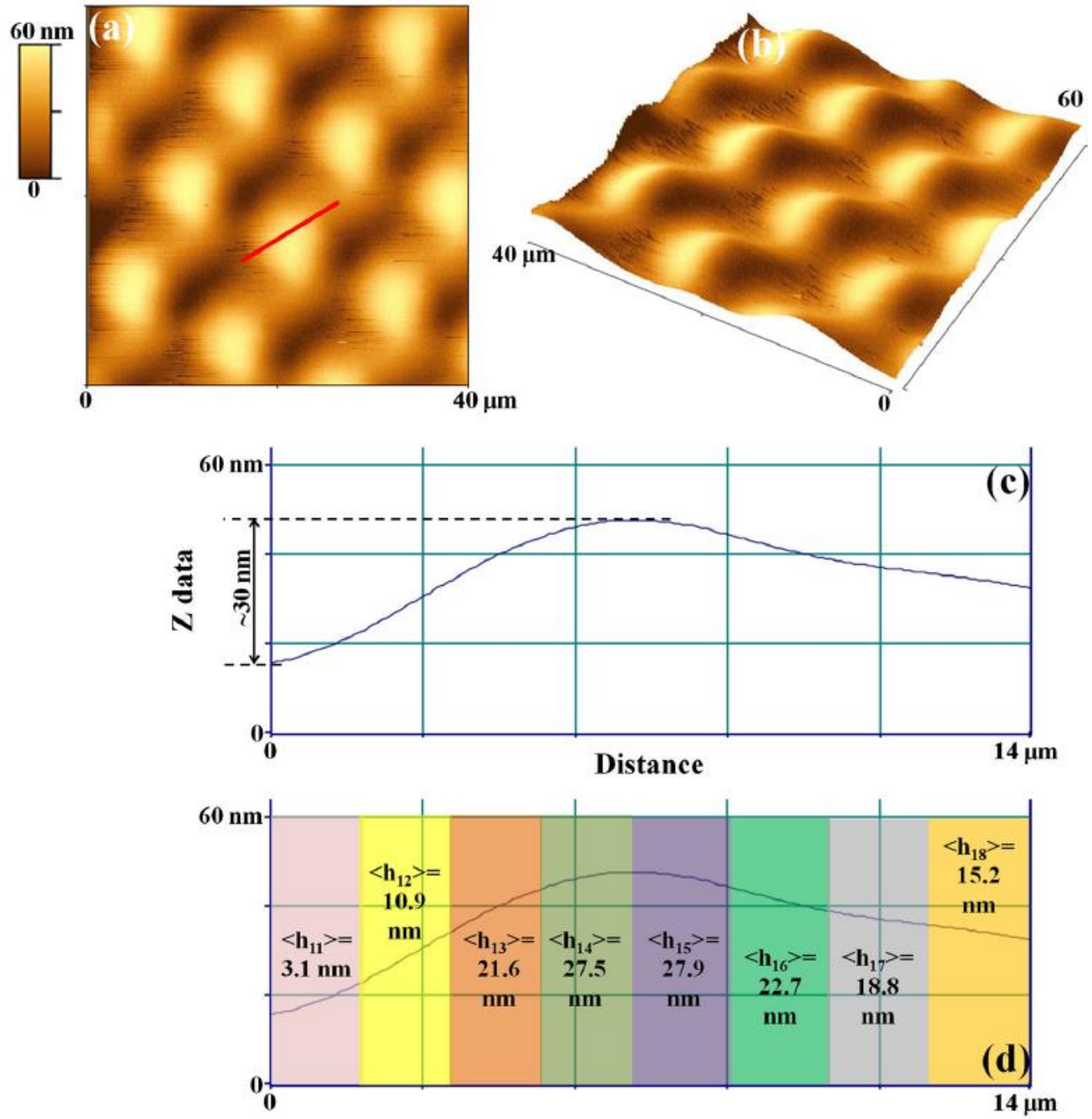

Fig. 4 **a** Two-dimensional AFM scan (40 µm × 40 µm) of the 40 nm-thick Au film deposited through the lithographic mask in oblique condition ($\alpha = 42°$). **b** Three-dimensional reconstruction of the AFM image in (**a**). **c** Cross-line profile of a Au square corresponding to the *red line* in (**a**). From this asymmetric cross-line profile, from the center to the edges the square is divided in height regions assigning to each region an effective height $\langle h_{ij} \rangle$ (**d**)

Superlattices and Microstructures 113 (2018) 430–441

Contents lists available at ScienceDirect

Superlattices and Microstructures

journal homepage: www.elsevier.com/locate/superlattices

Roughness evolution in dewetted Ag and Pt nanoscale films

F. Ruffino*, M.G. Grimaldi

Dipartimento di Fisica e Astronomia Università di Catania and MATIS CNR-IMM, Via S. Sofia 64, 95123 Catania, Italy

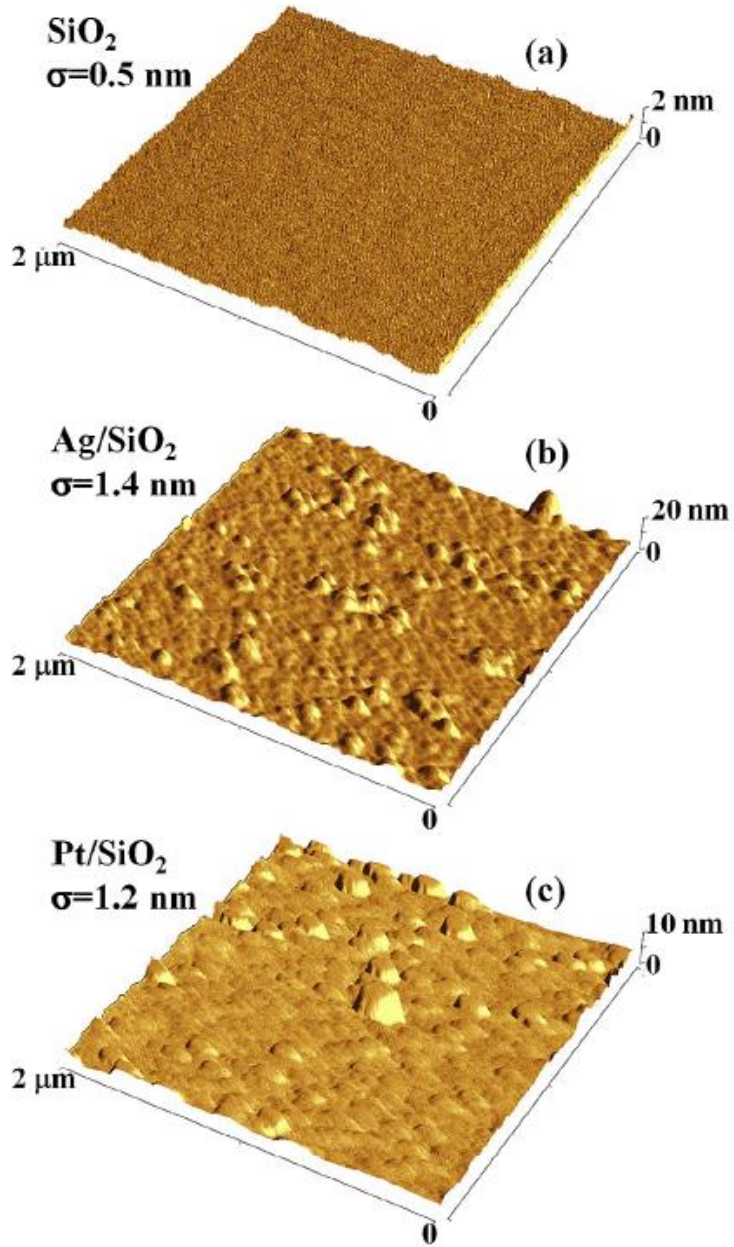

Fig. 1. Representative three-dimensional AFM images (2 μm × 2 μm) of: (a) the bare SiO_2 surface, (b) the surface of 15 nm-thick Ag film deposited on the SiO_2 surface, (c) the surface of 15 nm-thick Pt film deposited on the SiO_2 surface. Each image is accompained by the corresponding value of the roughness σ.

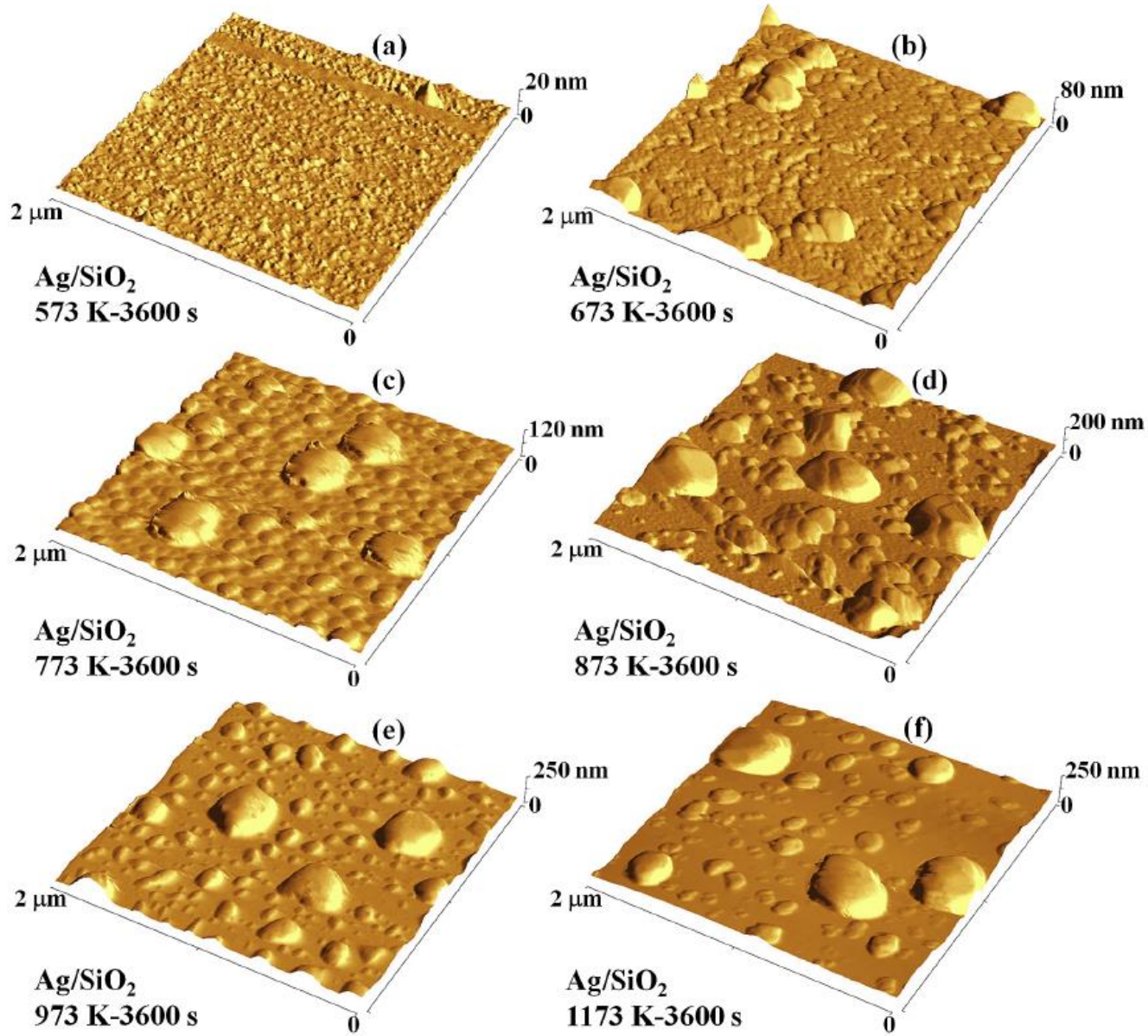

Fig. 2. Representative three-dimensional AFM images (2 μm × 2 μm) of the 15 nm-thick Ag film deposited on the SiO_2 surface and thermally processed at: (a) 573 K-3600 s, (b) 673 K-3600 s, (c) 773 K-3600 s, (d) 873 K-3600 s, (e) 973 K-3600 s, (f) 1173 K-3600 s. These images allow to follow the evolution of the Ag film morphology versus the annealing temperature.

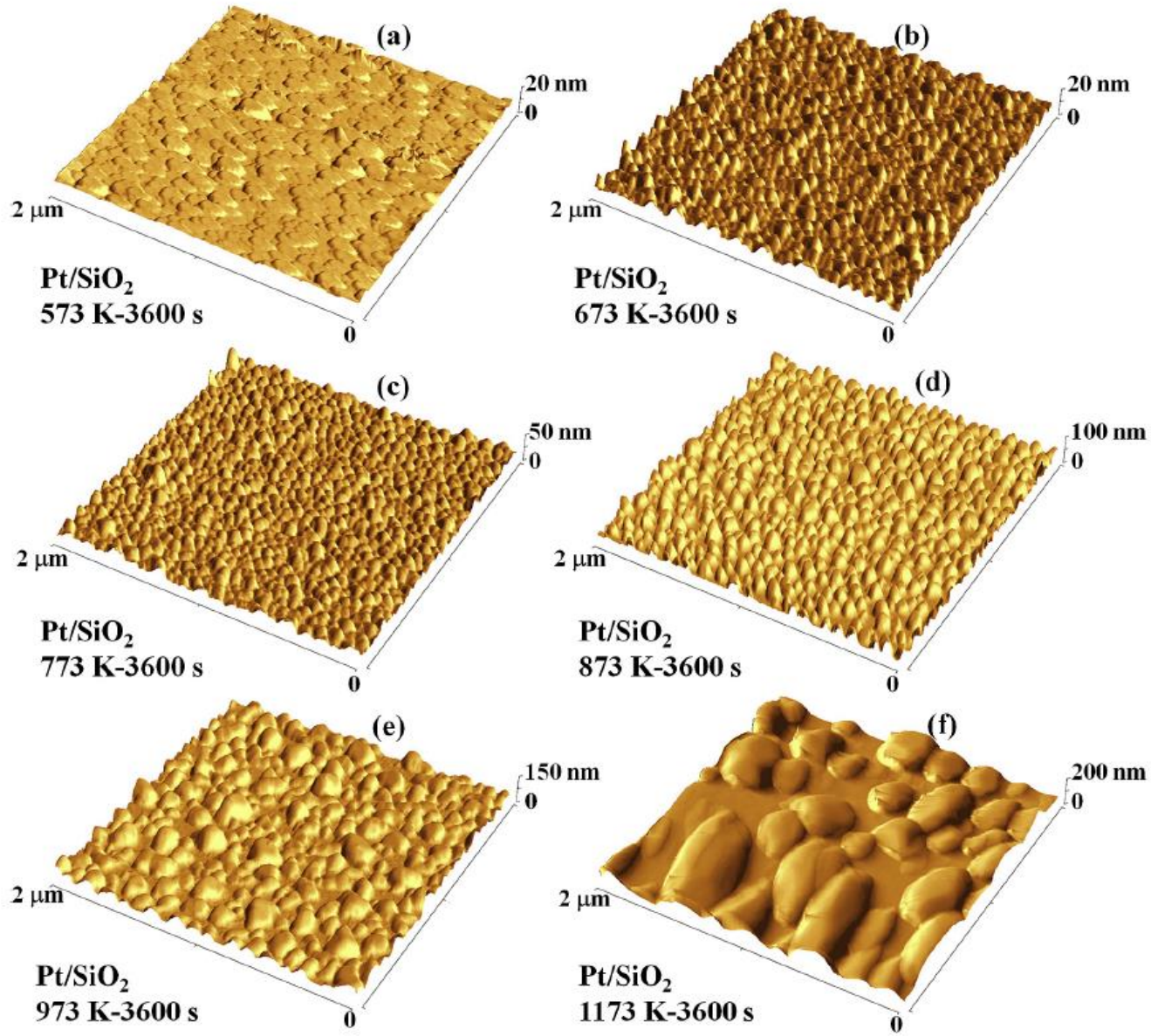

Fig. 3. Representative three-dimensional AFM images (2 μm × 2 μm) of the 15 nm-thick Pt film deposited on the SiO_2 surface and thermally processed at: (a) 573 K-3600 s, (b) 673 K-3600 s, (c) 773 K-3600 s, (d) 873 K-3600 s, (e) 973 K-3600 s, (f) 1173 K-3600 s. These images allow to follow the evolution of the Pt film morphology versus the annealing temperature.

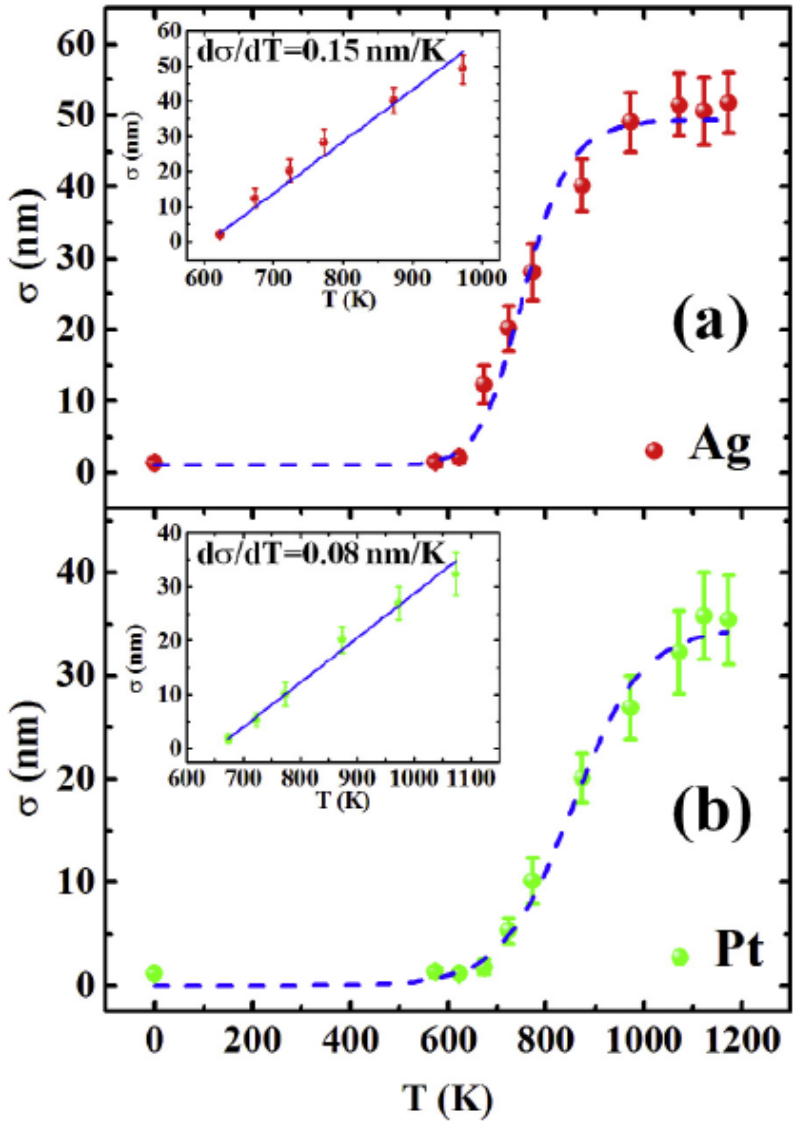

Fig. 4. Plots of the roughness σ versus the annealing temperature T when fixed the annealing time t = 3600 s, for the 15 nm-thick Ag film (a) and the 15 nm-thick Pt film (b). The insets report σ versus T restricted to the linear regions and the blue lines represent the corresponding linear fits of the experimental data.

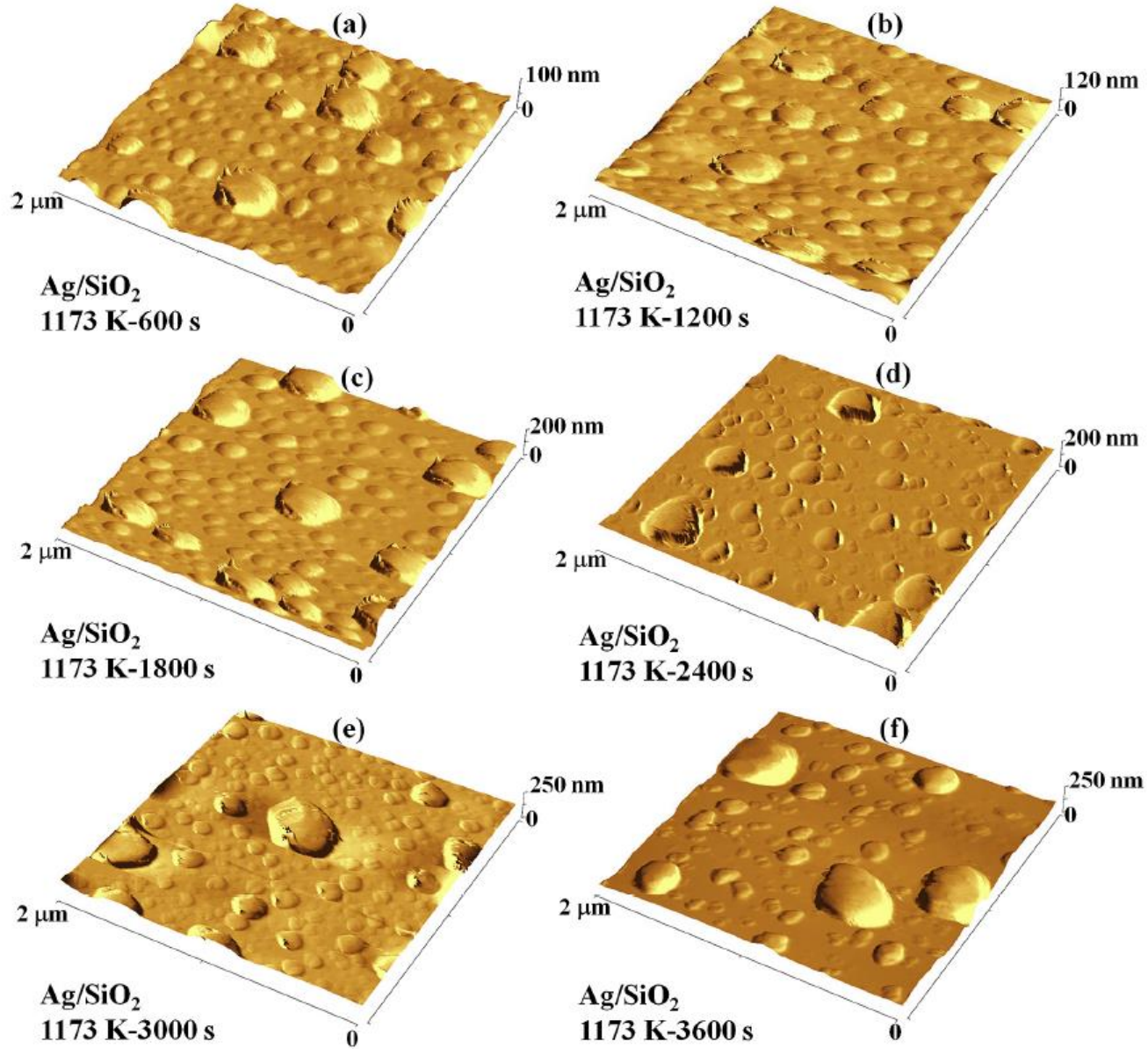

Fig. 5. Representative three-dimensional AFM images (2 μm × 2 μm) of the 15 nm-thick Ag film deposited on the SiO_2 surface and thermally processed at: (a) 1173 K-600 s, (b) 1173 K-1200 s, (c) 1173 K-1800 s, (d) 1173 K-2400 s, (e) 1173 K-3000 s, (f) 1173 K-3600 s. These images allow to follow the evolution of the Ag film morphology versus the annealing time.

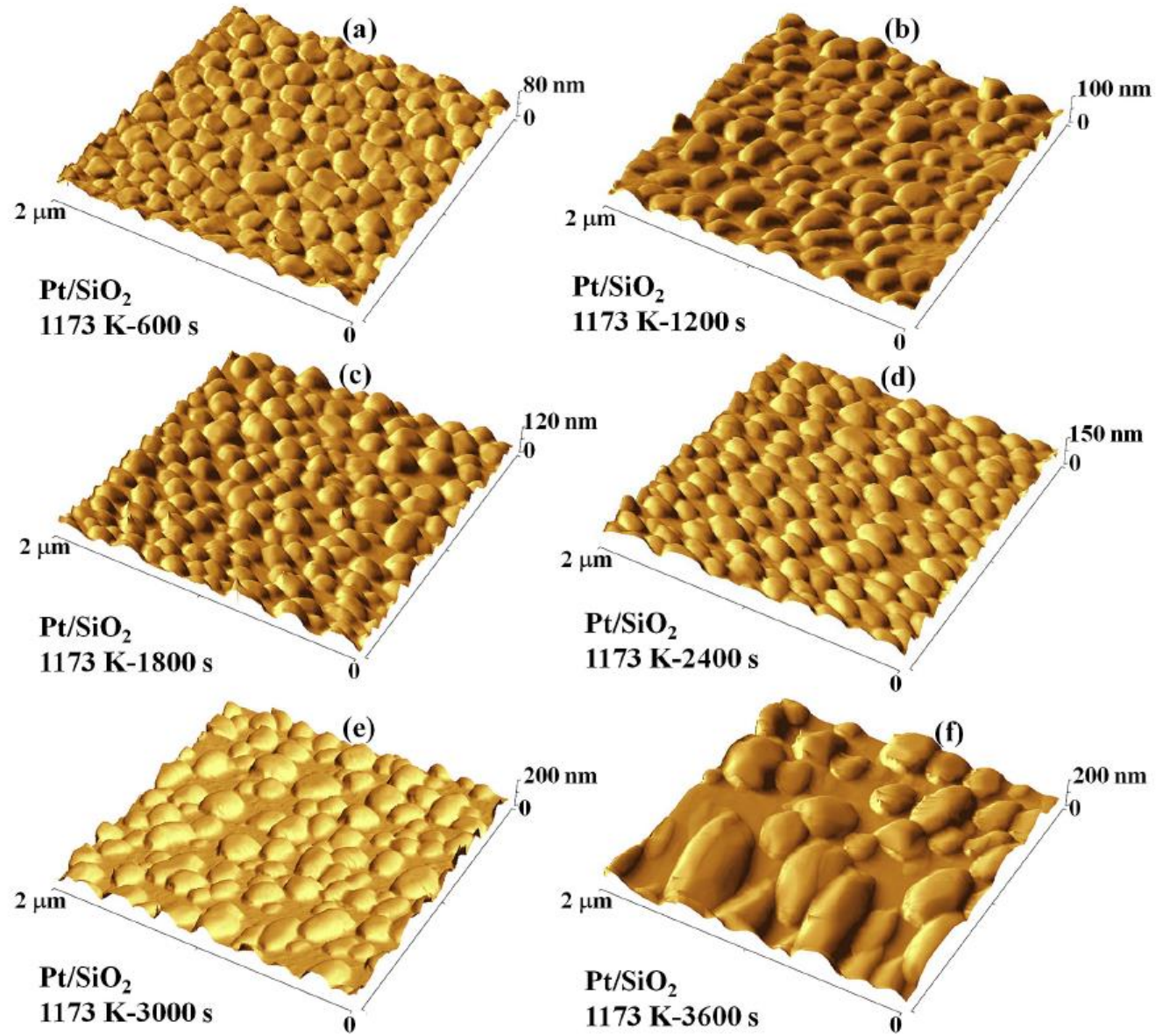

Fig. 6. Representative three-dimensional AFM images (2 μm × 2 μm) of the 15 nm-thick Pt film deposited on the SiO_2 surface and thermally processed at: (a) 1173 K-600 s, (b) 1173 K-1200 s, (c) 1173 K-1800 s, (d) 1173 K-2400 s, (e) 1173 K-3000 s, (f) 1173 K-3600 s. These images allow to follow the evolution of the Pt film morphology versus the annealing time.

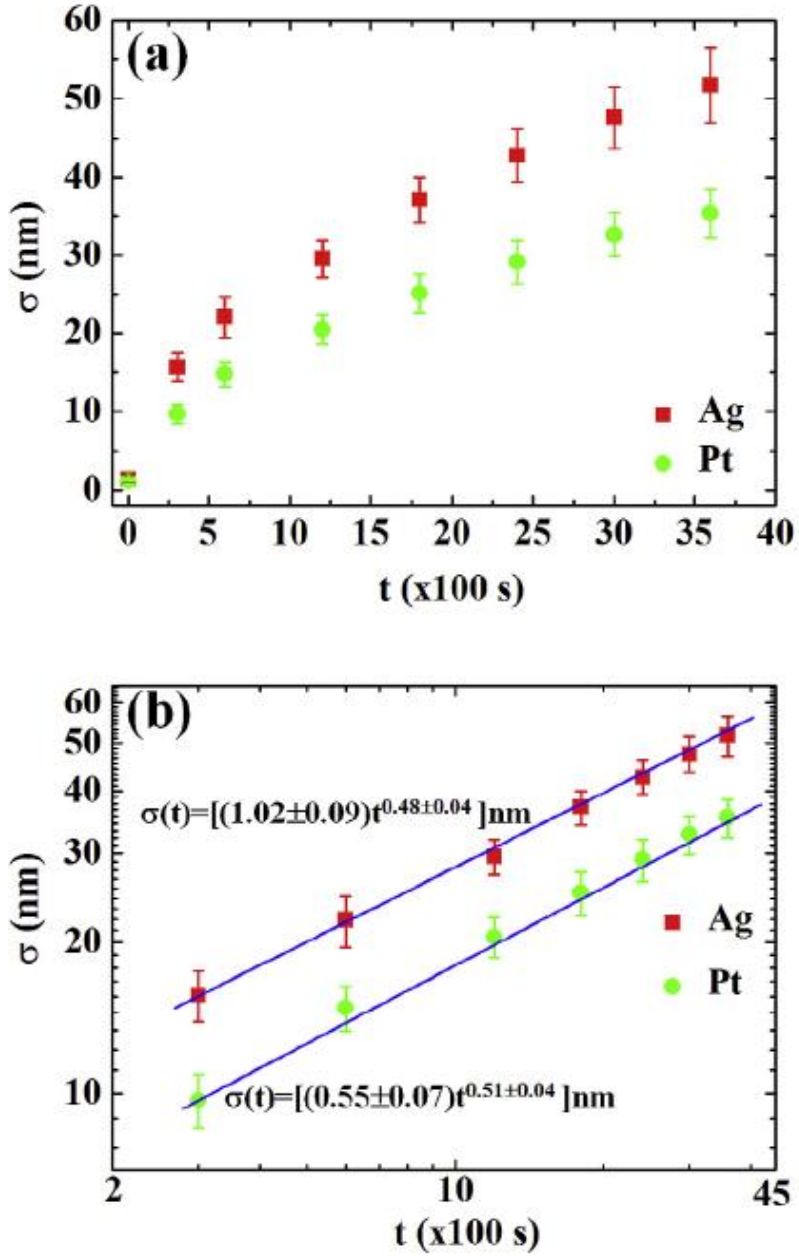

Fig. 7. (a) Plots of the roughness σ versus the annealing time t when fixed the annealing temperature T = 1173 K, for the 15 nm-thick Ag film and the 15 nm-thick Pt film. (b) Reports the same experimental data (apart the value for t = 0 s) plotted in Log-Log scale and the continuous lines indicate the fit of the experimental data by $\sigma(t) = \alpha t^{\beta}$ from which values for the fitting parameters α and β are extracted.

Solid State Communications 225 (2016) 1–6

Contents lists available at ScienceDirect

Solid State Communications

journal homepage: www.elsevier.com/locate/ssc

Nanoscale electrical characteristics of metal (Au, Pd)–graphene–metal (Cu) contacts

F. Ruffino [a,b,*], G. Meli [a], M.G. Grimaldi [a,b]

[a] Dipartimento di Fisica ed Astronomia-Università di Catania, via S. Sofia 64, 95123 Catania, Italy
[b] MATIS IMM-CNR, via S. Sofia 64, 95123 Catania, Italy

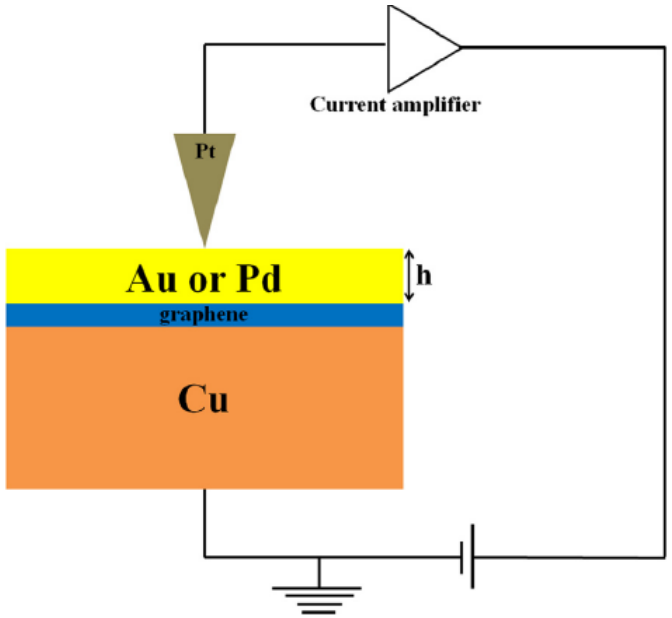

Fig. 2. Picture of the analyzed samples and conductive atomic force microscopy measurement setup configuration.

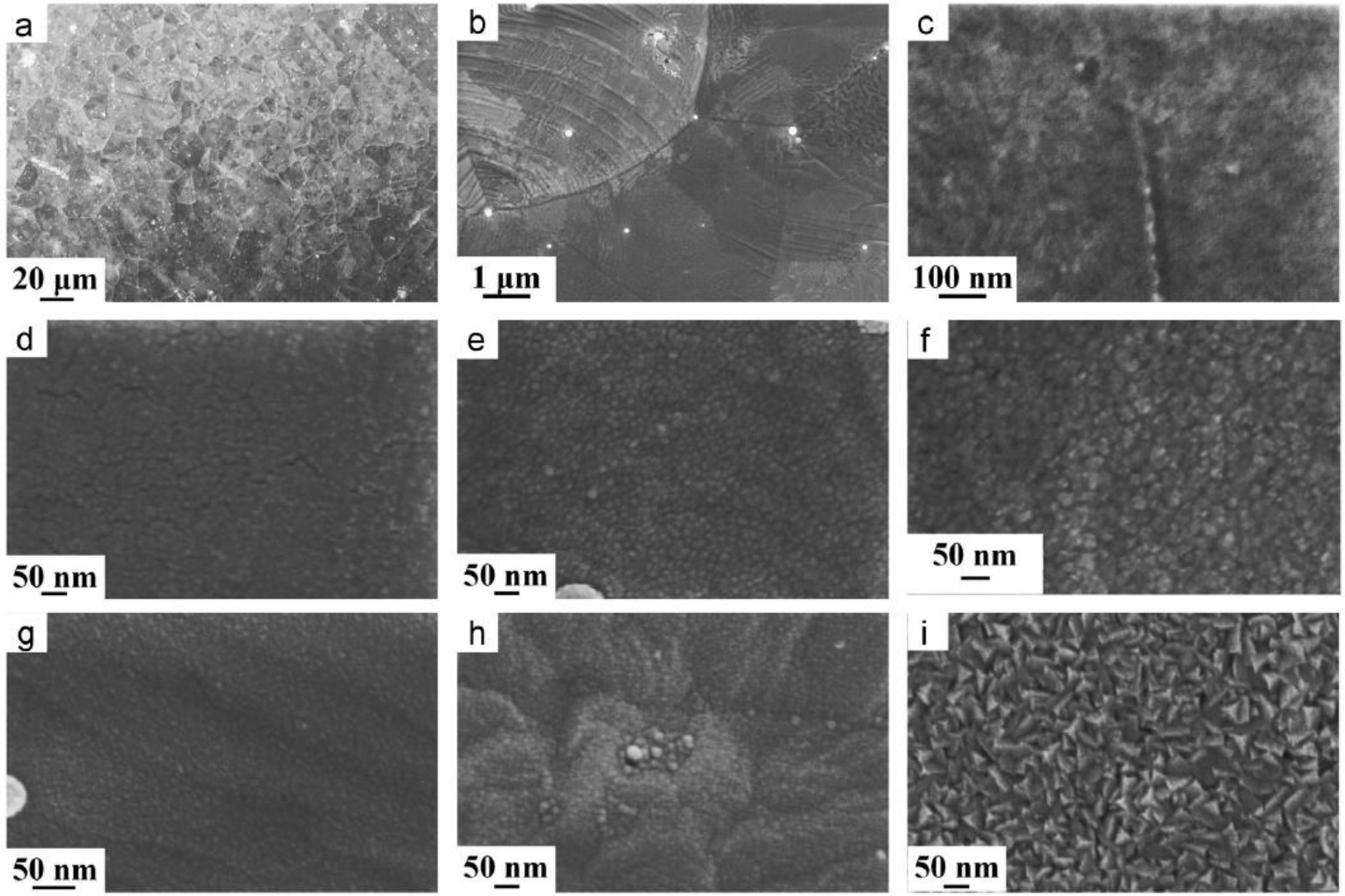

Fig. 3. Representative scanning electron microscopy images of: (a)–(c) graphene/Cu surface at different magnifications, (d)–(f) Au films deposited on the graphene/Cu surface with thickness of 5 nm (d), 25 nm (e) and 50 nm (f), (g)–(i) Pd films deposited on the graphene/Cu surface with thickness of 5 nm (g), 25 nm (h) and 50 nm (i).

Table 1

W_M: metal work-function, W_G: free-standing graphene work-function (4.48 eV) and graphene work-function when in contact with a specific metal. Adapted from [18].

	Gr	Pd	Cu	Au	Pt
W_M(eV)		5.67	5.22	5.54	6.13
W_G(eV)	4.48	4.03	4.40	4.74	4.87

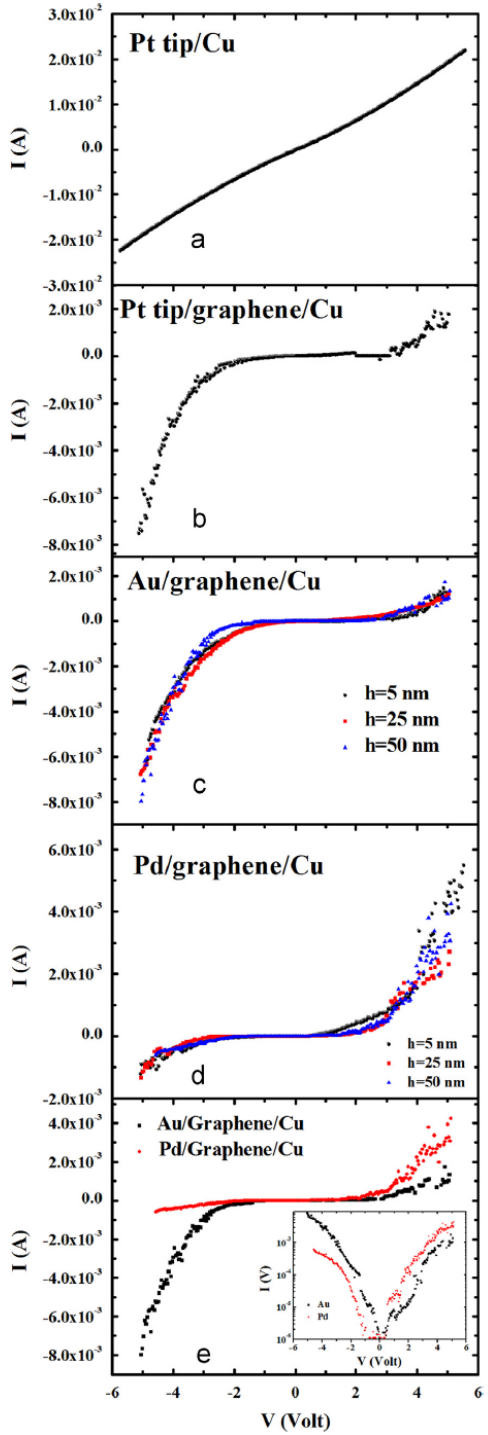

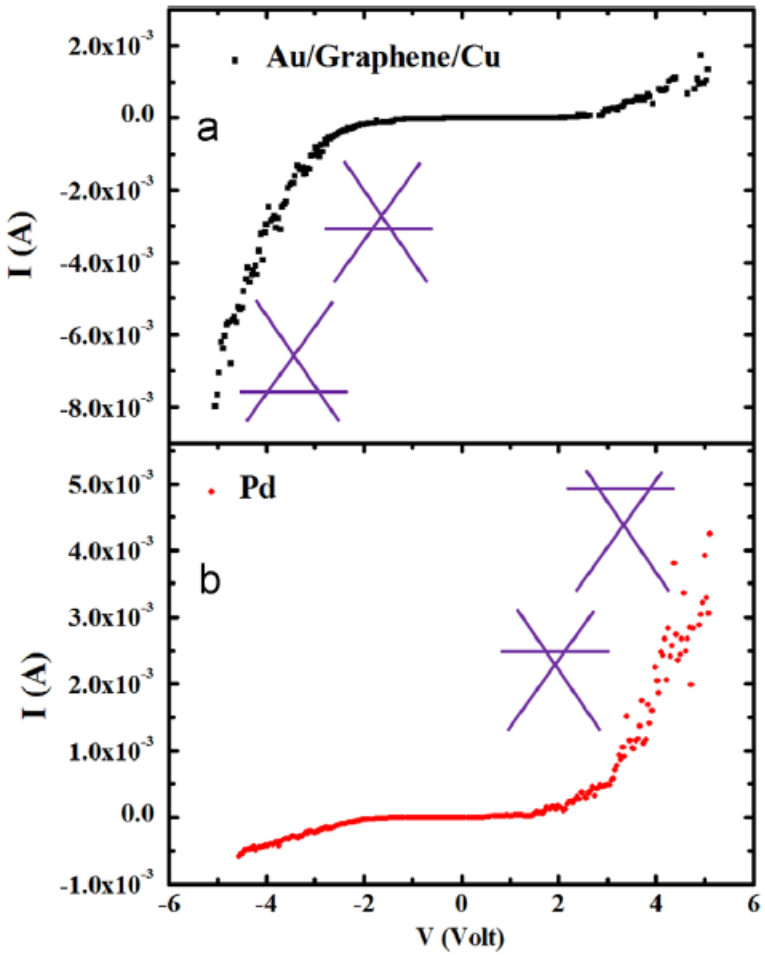

Applied Surface Science 359 (2015) 637–642

Contents lists available at ScienceDirect

Applied Surface Science

journal homepage: www.elsevier.com/locate/apsusc

Emerging interface dipole *versus* screening effect in copolymer/metal nano-layered systems

V. Torrisi[a,*], F. Ruffino[b,c], A. Liscio[d], M.G. Grimaldi[b,c], G. Marletta[a]

[a] *Laboratory for Molecular Surfaces and Nanotechnology (LAMSUN), Department of Chemical Sciences, University of Catania, Viale A. Doria 6, 95125, Catania, Italy*
[b] *Dipartimento di Fisica ed Astronomia-Università di Catania, via S. Sofia 64, 95123 Catania, Italy*
[c] *MATIS IMM-CNR, via S. Sofia 64, 95123 Catania, Italy*
[d] *Istituto per la Sintesi e la Fotoreattività CNR, via Gobetti 101, 40129, Bologna, Italy*

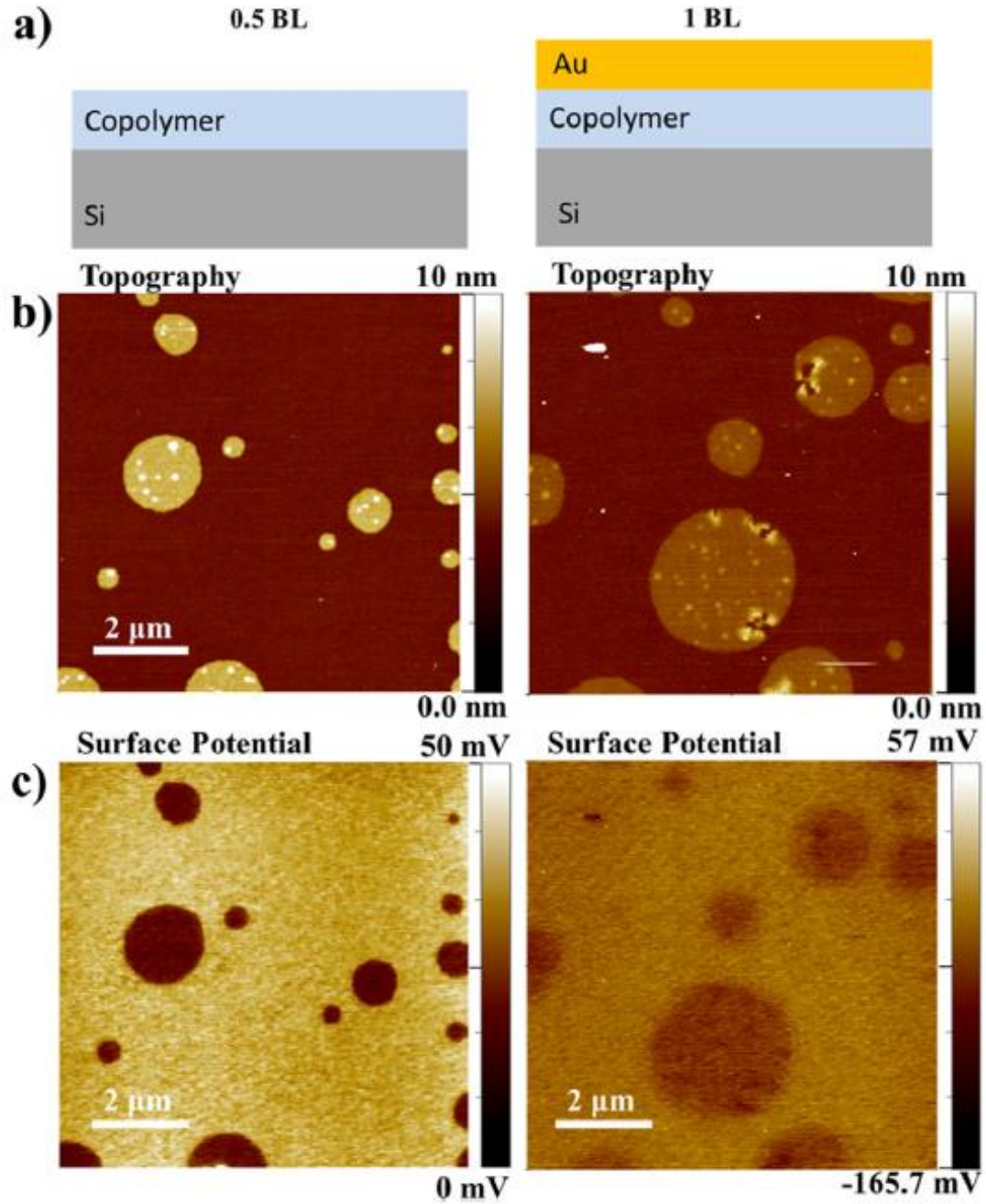
a)
0.5 BL
1 BL
Au
Copolymer
Copolymer
Si
Si
b)
Topography
10 nm
Topography
10 nm
2 µm
0.0 nm
0.0 nm
c)
Surface Potential
50 mV
Surface Potential
57 mV
2 µm
2 µm
0 mV
-165.7 mV

AFM: surface roughness

ence surface. Films grown under nonequilibrium condition are expected to develop self-affine surfaces [7, 14], whose rms widths scale with time t and the length L sampled as [15]

$$\sigma(L,t) = L^{\alpha} F\left(t/L^{\alpha/\beta}\right) \tag{1}$$

where $\sigma(L) \propto L^{\alpha}$ for $t/L^{\alpha/\beta} \to \infty$ and $\sigma(t) \propto t^{\beta}$ for $t/L^{\alpha/\beta} \to 0$. The parameter $0 < \alpha < 1$ is defined as the roughness exponent [16], and the parameter, β, as the growth exponent. Actual self-affine surfaces are characterized by an upper horizontal cutoff to scaling, or correlation length, ξ, beyond which the surface width no longer scales as L^{α}, and eventually reaches a saturation

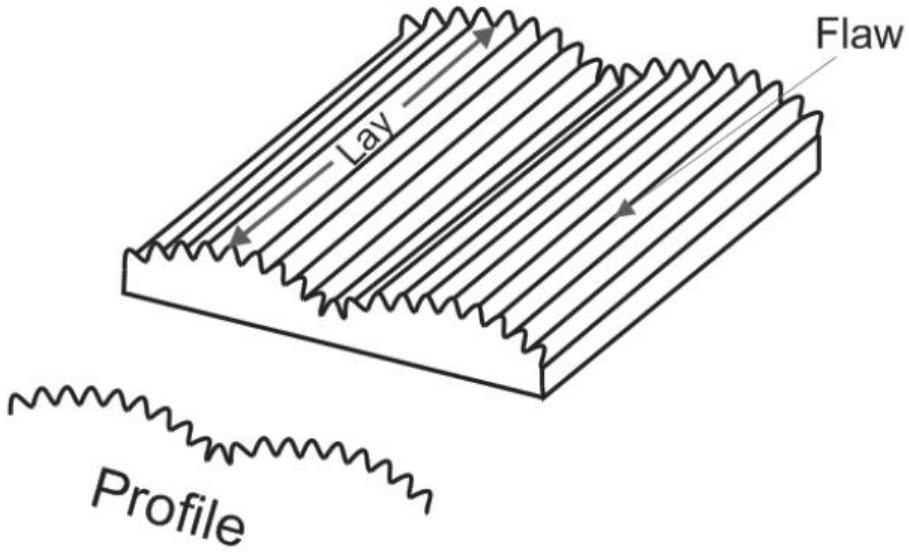

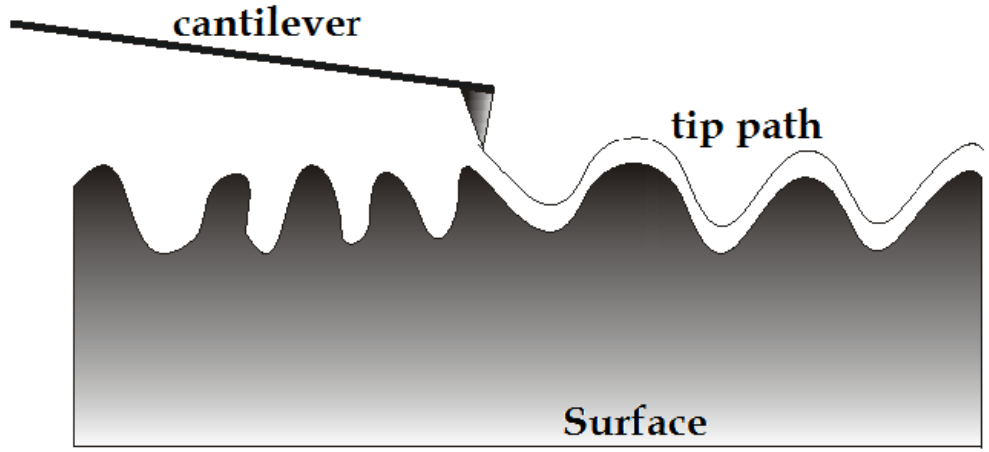

value, σ. Implicit in Eq. 1 is a correlation length which increases with time as $\xi \propto t^{1/z}$, where $z = \alpha/\beta$ is the dynamic scaling exponent.

In thin films deposition methodologies in which the film thickness, h, is proportional to the time of deposition, t, then, in the asymptotical limits,

$$\sigma(h) = ah^{\beta} \tag{2}$$

$$\xi(h) = bh^{1/z} \tag{3}$$

where a and b are the opportune proportionality constants.

The global surface morphology thus proceeds to a steady growth with the evolution of vertical roughening and lateral coarsening. Two correlation lengths are assigned to describe the interface growth process: the mean surface height fluctuations σ, which is a measure of the vertical interface roughness, and the lateral correlation length ξ, which characterizes the coarsening size. In particular, the roughness function is defined by[30]

$$\sigma = \langle z(x,y)^2 \rangle^{1/2} = \langle [h(x,y) - \langle h(x,y) \rangle]^2 \rangle^{1/2}, \quad (6)$$

where $h(x,y)$ is the height function and $\langle \cdots \rangle$ is the spatial average over a planar reference surface. The roughness σ of a real self-affine surface must saturate at large length scales, and the correlation length ξ is the horizontal cutoff associated with the saturation value of σ. For a growing film, the time evolution of the saturated σ is characterized by the "growth" exponent[30] β,

$$\sigma \propto \langle h \rangle^{\beta}. \quad (7)$$

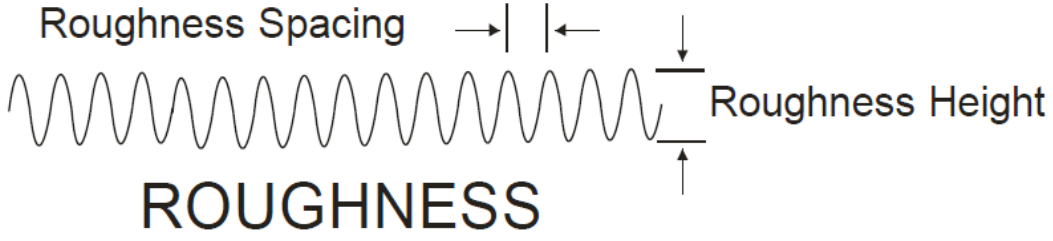

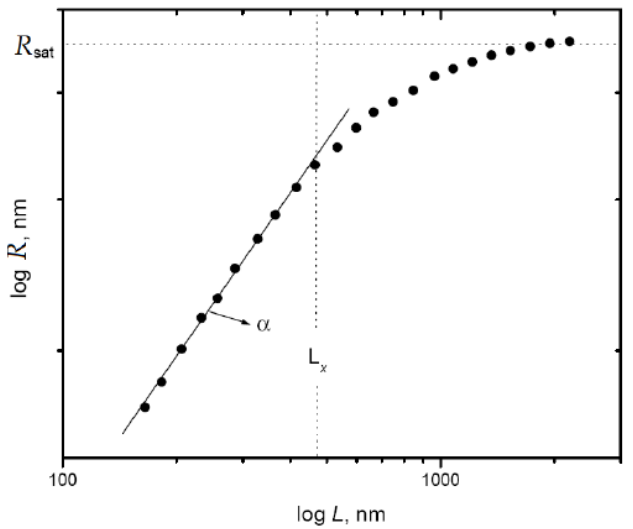

Fig. 25. For self-affine surfaces, the slope of the unsaturated region of roughness is the roughness exponent (Cruz T.G.S., 2002).

JOURNAL OF APPLIED PHYSICS **107**, 104321 (2010)

Atomic force microscopy study of the growth mechanisms of nanostructured sputtered Au film on Si(111): Evolution with film thickness and annealing time

F. Ruffino[a)] and M. G. Grimaldi
Dipartimento di Fisica e Astronomia, Università di Catania, via S. Sofia 64, 95123 Catania, Italy and CNR-IMM MATIS, via S. Sofia 64, 95123 Catania, Italy

(Received 19 January 2010; accepted 15 April 2010; published online 26 May 2010)

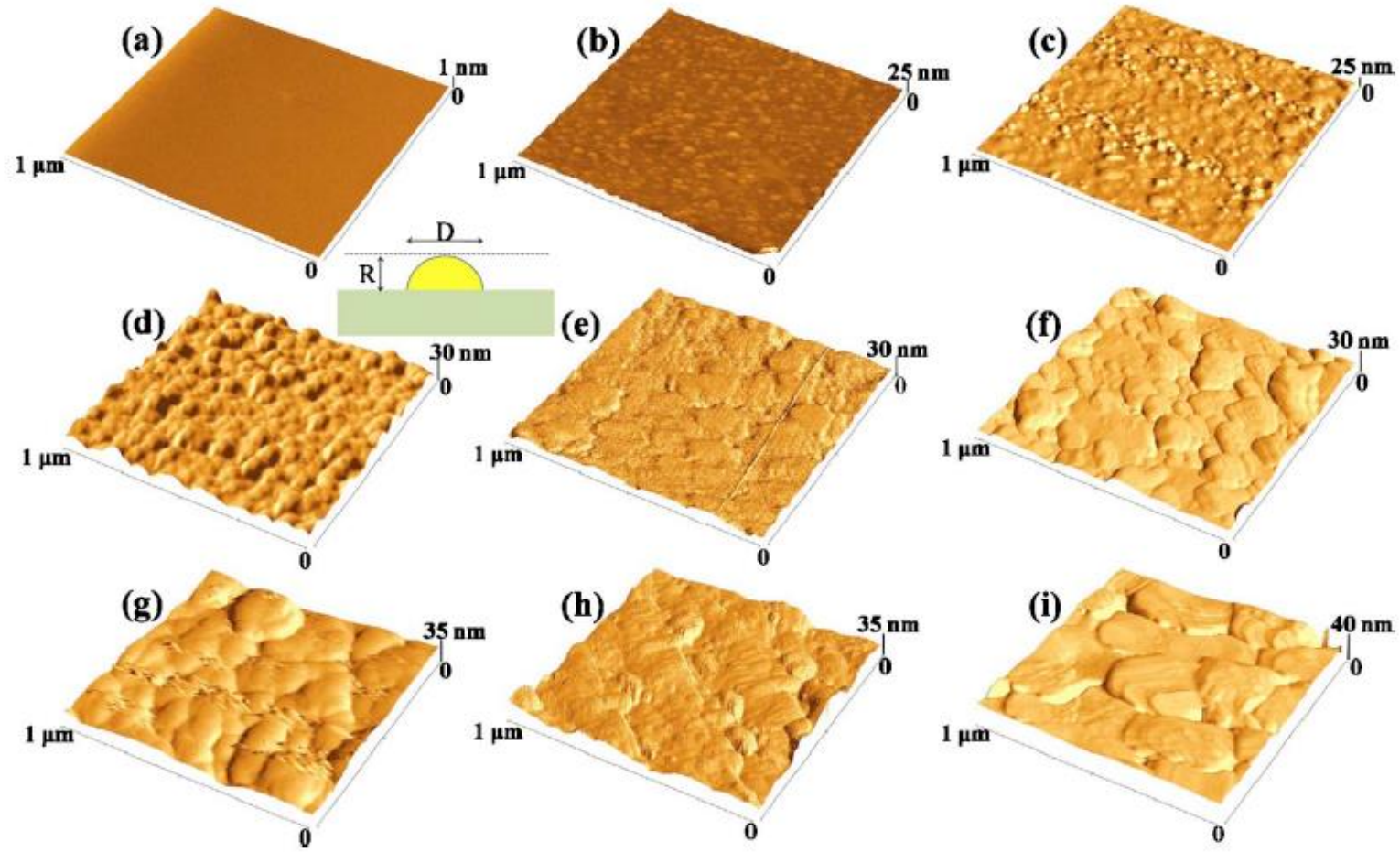

FIG. 1. (Color online) (a) 1×1 μm^2 AFM image of the Si(111) substrate; 1×1 μm^2 AFM images of the Si(111) substrate sputter-deposited with Au of different thickness h: (b) $h=1.7\times10^{17}$ Au/cm^2, (c) $h=2.1\times10^{17}$ Au/cm^2, (d) $h=3.0\times10^{17}$ Au/cm^2, (e) $h=5.2\times10^{17}$ Au/cm^2, (f) $h=6.8\times10^{17}$ Au/cm^2, (g) $h=7.7\times10^{17}$ Au/cm^2, (h) $h=9.4\times10^{17}$ Au/cm^2, and (i) $h=1.0\times10^{18}$ Au/cm^2. The inset shows a schematic of the horizontal, D, and vertical, R, dimensions of the Au clusters.

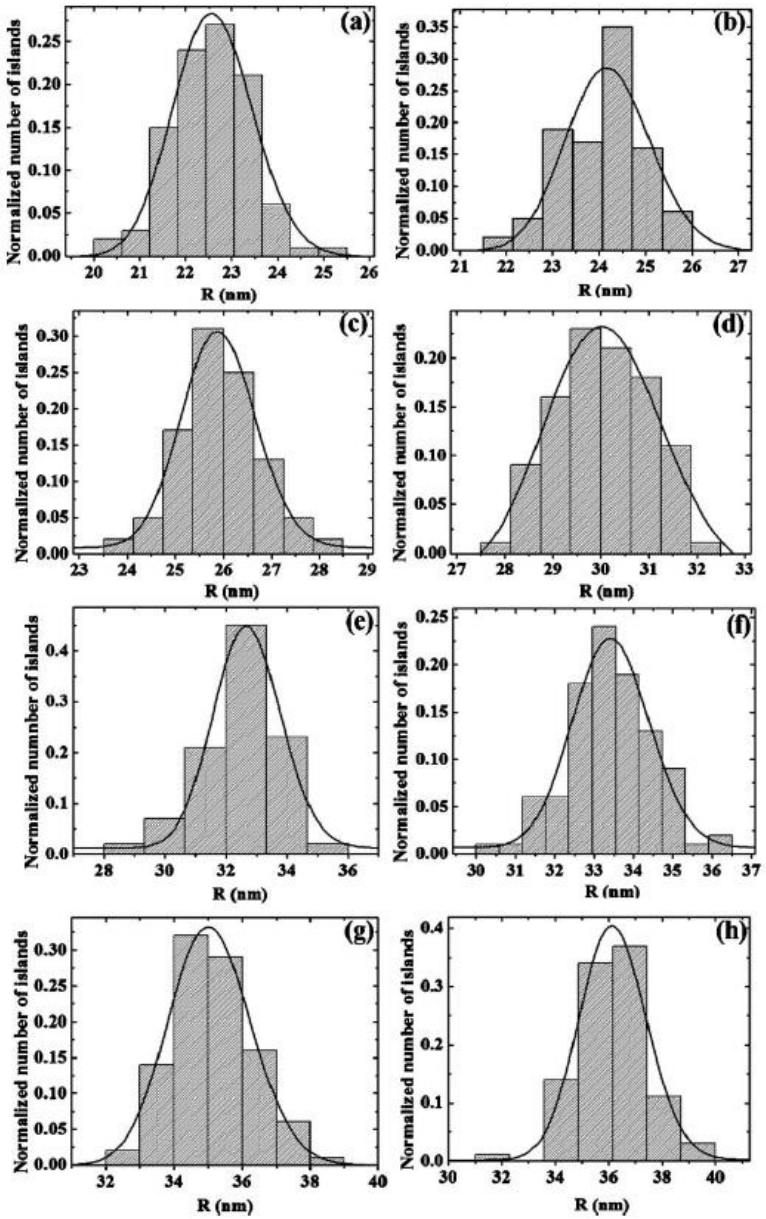

FIG. 2. Distributions of the clusters vertical size R for samples with different amount h of Au: (a) $h=1.7\times10^{17}$ Au/cm^2, (b) $h=2.1\times10^{17}$ Au/cm^2, (c) $h=3.0\times10^{17}$ Au/cm^2, (d) $h=5.2\times10^{17}$ Au/cm^2, (e) $h=6.8\times10^{17}$ Au/cm^2, (f) $h=7.7\times10^{17}$ Au/cm^2, (g) $h=9.4\times10^{17}$ Au/cm^2, and (h) $h=1.0\times10^{18}$ Au/cm^2. The continuous lines are the fits by the log-normal function.

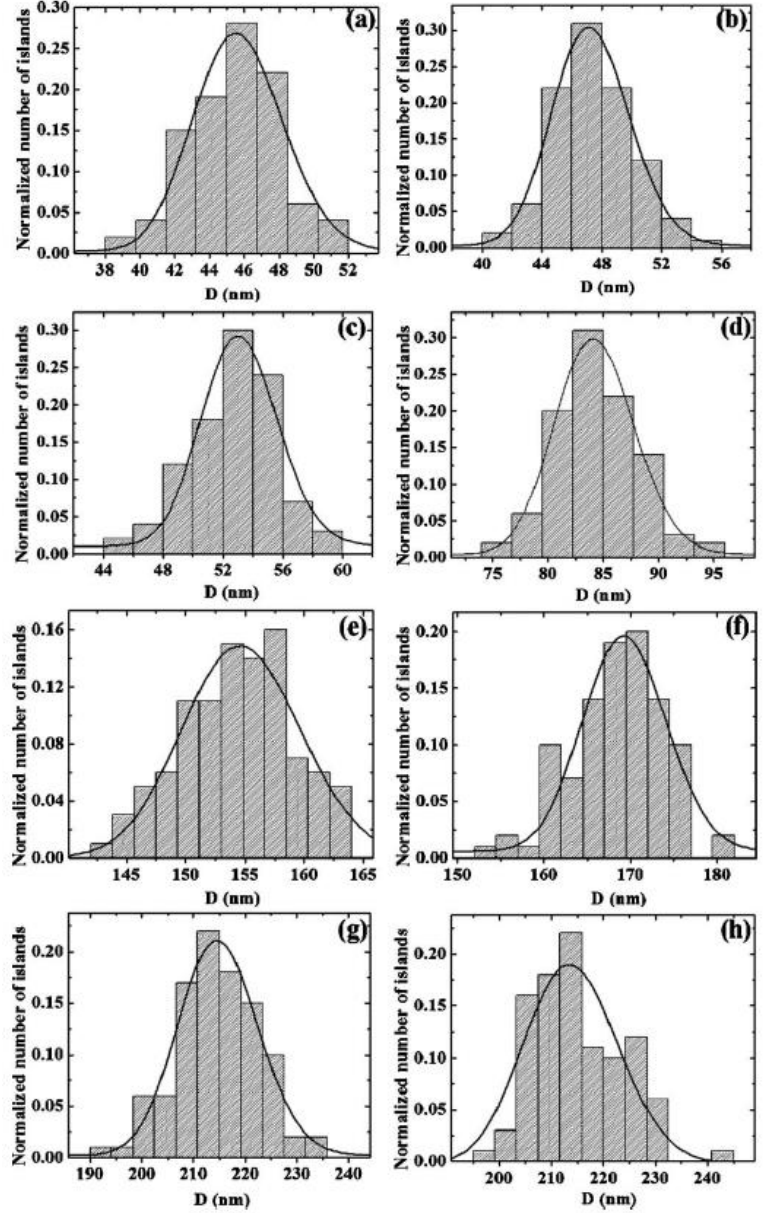

FIG. 3. Distributions of the clusters vertical size D for samples with different amount h of Au: (a) $h=1.7\times10^{17}$ Au/cm^2, (b) $h=2.1\times10^{17}$ Au/cm^2, (c) $h=3.0\times10^{17}$ Au/cm^2, (d) $h=5.2\times10^{17}$ Au/cm^2, (e) $h=6.8\times10^{17}$ Au/cm^2, (f) $h=7.7\times10^{17}$ Au/cm^2, (g) $h=9.4\times10^{17}$ Au/cm^2, and (h) $h=1.0\times10^{18}$ Au/cm^2. The continuous lines are the fits by the log-normal function.

Stage 1: Nucleation

Stage 2: Lateral growth

Stage 3: Coalescence

Stage 4: Vertical growth

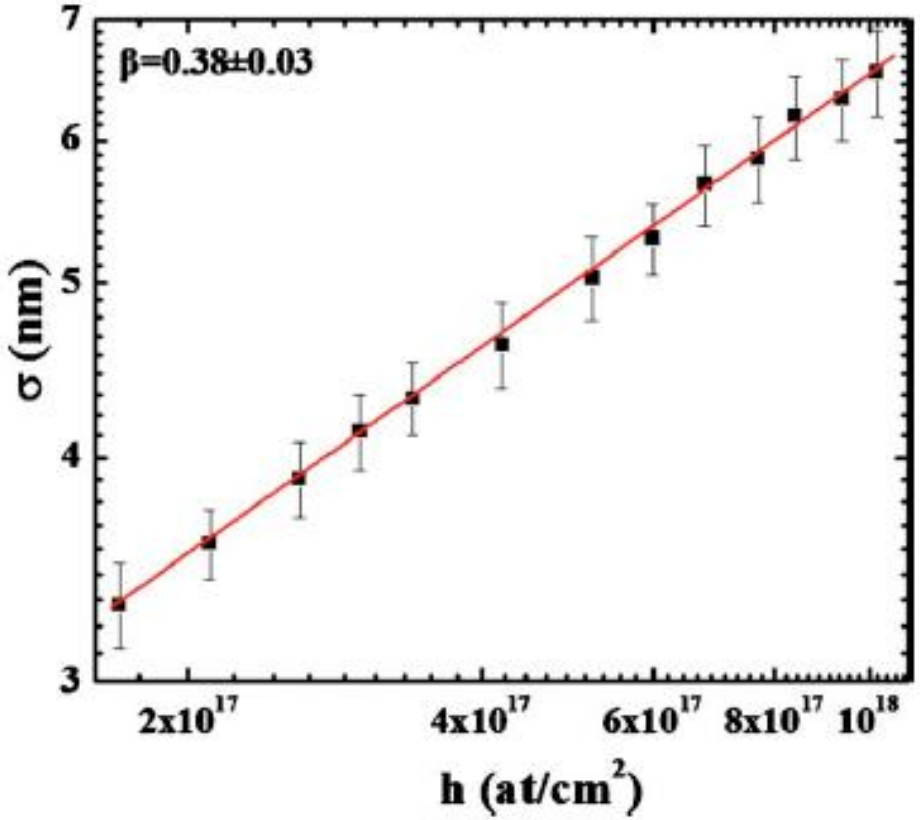

Chemical Physics Letters 639 (2015) 120–125

Contents lists available at ScienceDirect

Chemical Physics Letters

journal homepage: www.elsevier.com/locate/cplett

Quantitative evaluation of surface topographical changes of Au thin films after DNA immobilization

S. Spampinato[a], G. Cacciato[a,b], M. Zimbone[b,*], F. Ruffino[a,b], M.G. Grimaldi[a,b]

[a] *Dipartimento di Fisica ed Astronomia – Università di Catania, via S. Sofia 64, 95123, Catania, Italy*
[b] *IMM-CNR, via S. Sofia 64, 95123, Catania, Italy*

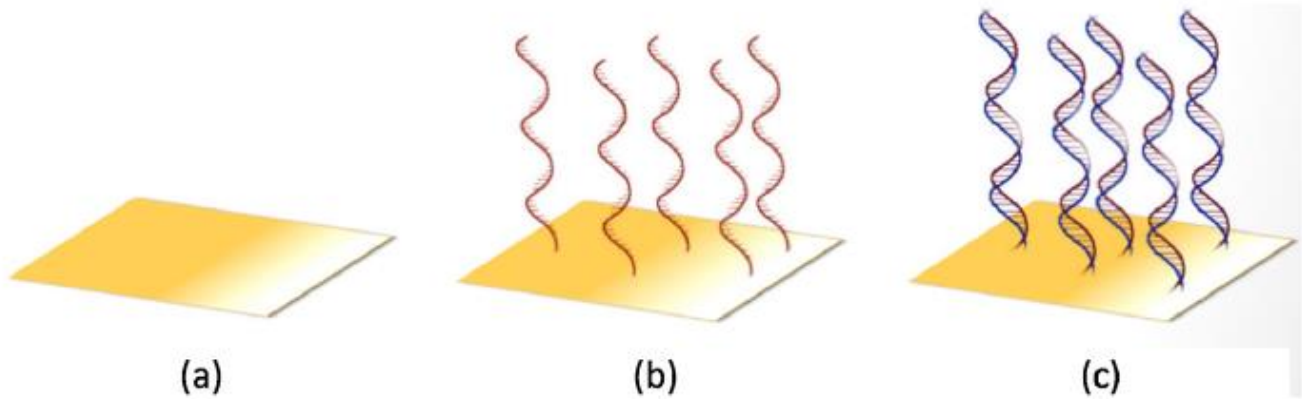

Figure 1. Schematic pictures of the analyzed samples: (a) bare Au surface, (b) Au surface after ssDNA immobilization, (c) Au surface after dsDNA hybridization.

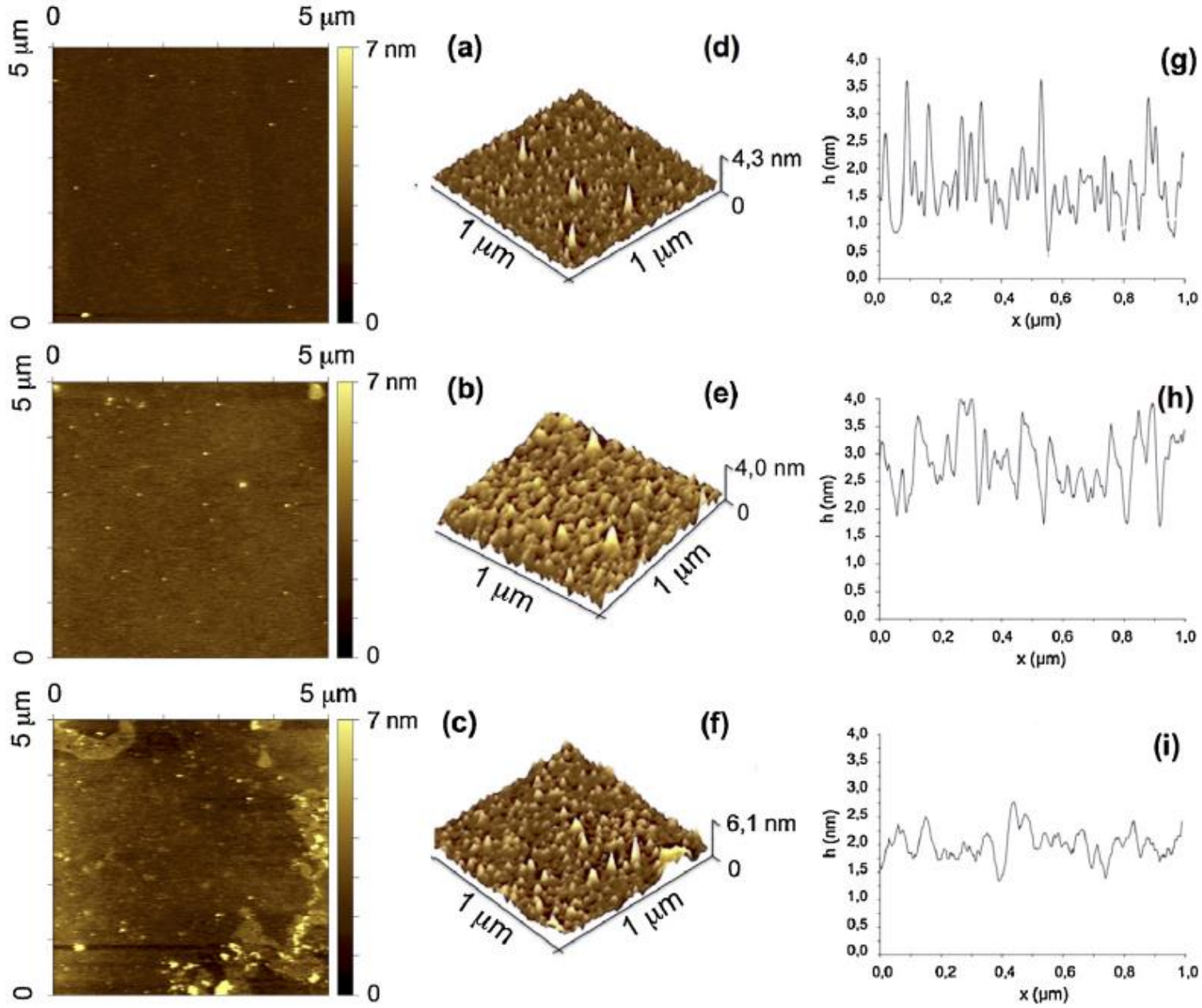

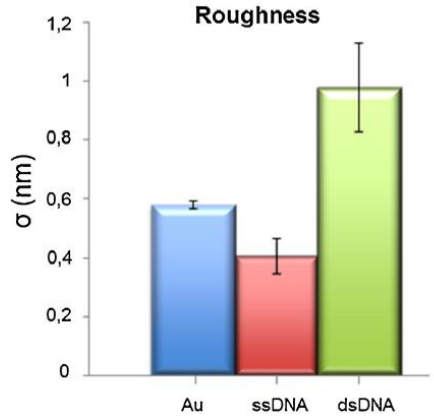

Figure 3. Calculated values for the roughness of the bare Au surface and after ssDNA immobilization and dsDNA hybridization.

Figure 2. (a)–(c) Representative 5 µm × 5 µm 2D AFM images corresponding to the bare Au surface (a), the Au surface after ssDNA immobilization (b), and the Au surface after dsDNA hybridization (c). (d)–(f) Representative 1 µm × 1 µm 3D AFM images corresponding to the bare Au surface (d), the Au surface after ssDNA immobilization (e), and the Au surface after dsDNA hybridization (f). (g)–(i) Representative cross-line section profiles of the corresponding 1 µm × 1 µm scan of the surfaces.

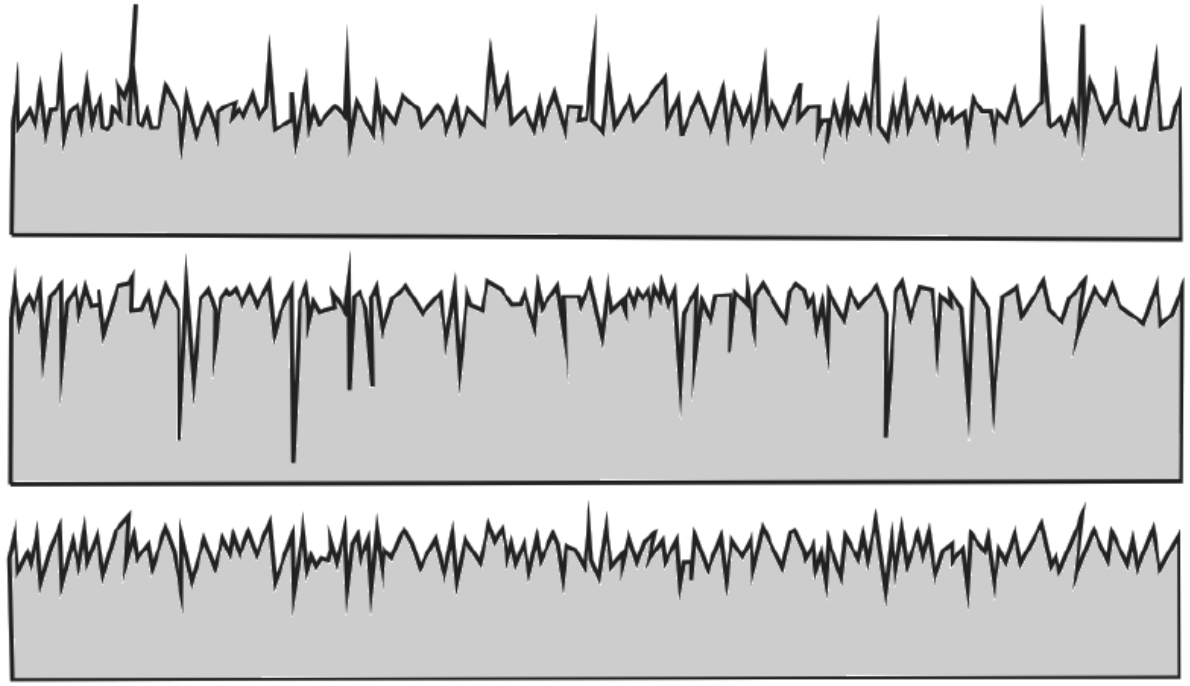

Fig. 13. Different profiles of surfaces, with the same roughness average (adapted from Predev, 2011).

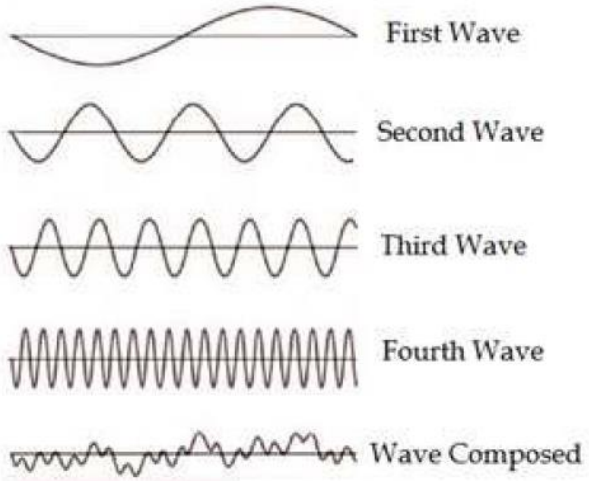

Fig. 26. Example of a wave decomposed by PSD. The sum of the four waves results in the composed wave (adapted from Freitas, A. C. P., 2010).

The power spectral density (PSD) is a complementary analysis of surface roughness which gives information related to parameters of the roughness height and spacing. The PSD is a parameter used in micrographs which relates the Fourier Transform (FT) with the root mean square roughness (RMS). The relationship between the PSD, FT and RMS is described by (Park, 2011):

$$PSD = FT^2 \tag{22}$$

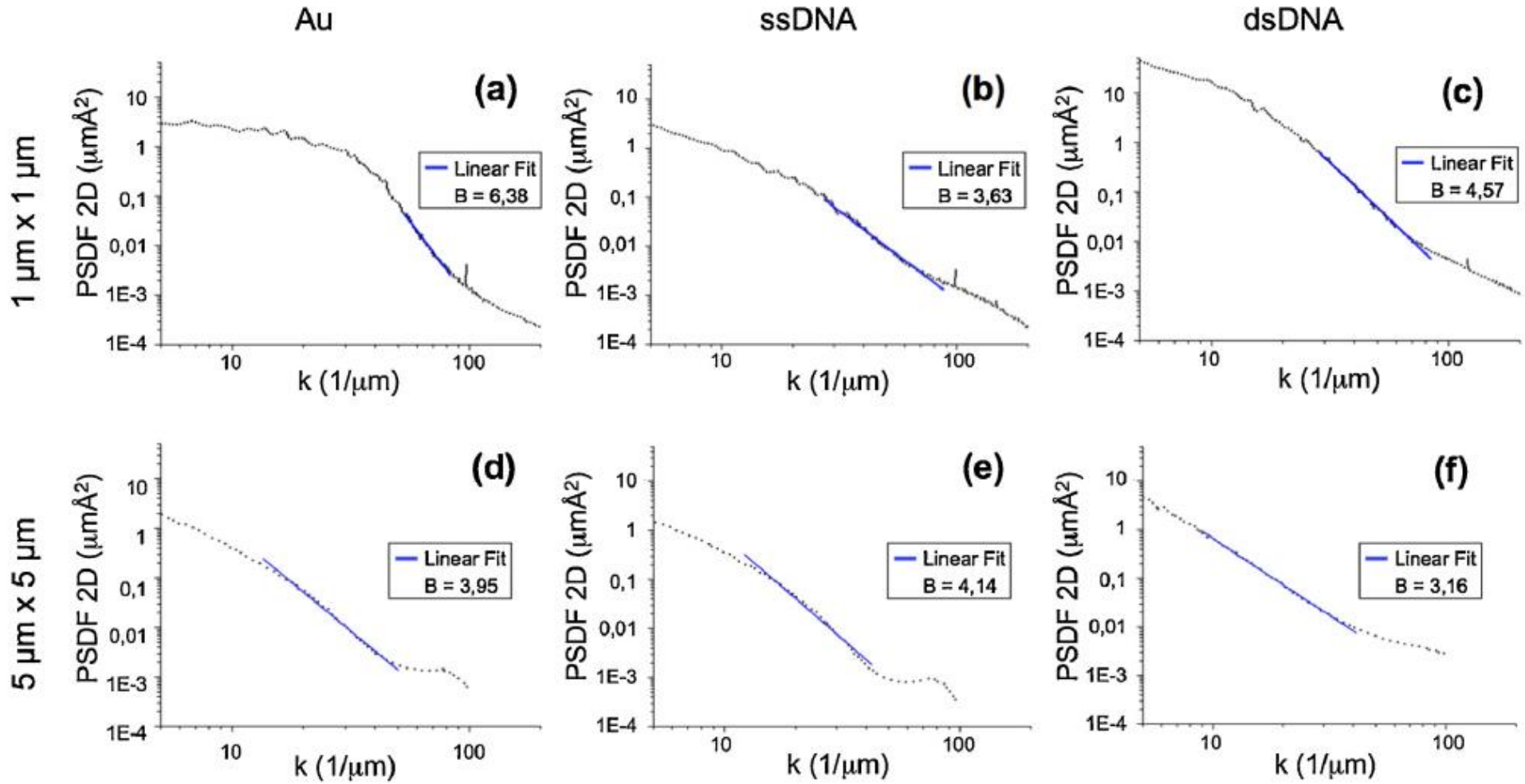

Figure 4. Representative two-dimensional PSD spectra for (a) the bare Au surface obtained by the analysis of 1 µm × 1 µm scans, (b) the Au surface after ssDNA immobilization and obtained by 1 µm × 1 µm scans, (c) the Au surface after dsDNA immobilization and obtained by 1 µm × 1 µm scans, (d) the bare Au surface and obtained by the analysis of 5 µm × 5 µm scans, (e) the Au surface after ssDNA immobilization and obtained by 5 µm × 5 µm scans, (f) the Au surface after dsDNA immobilization and obtained by 5 µm × 5 µm scans. The full lines are the fit of the linear regions.

However, the roughness σ of a surface might not correctly represent the anisotropy of the topography. In fact, for example, almost similar σ values can be found for surfaces containing either few high-amplitude features or many low-lying features. Thus, we evaluated the two-dimensional fractal dimension D_f for the examined surface.

Mathematically, a surface exhibits fractal behavior when the dimension is non-integer, having fractional values [40]. For real surfaces, the fractal dimension, D_f, is $2 \leq D_f \leq 3$ and a smooth surface has a D_f value near 2, and an increasing surface roughness, either by porosity and/or relief increments, should increase the D_f value without exceeding the value of 3 [41]. At nanometric scale, most surface structures of materials have complicated shapes and surface topography is generally quantified by the roughness. Such parameter is useful to describe the surface quality, but its values can be ambiguous because the surface topography is, in general, multiscaled [42]. More information can be achieved by using a fractal approach in which the fractal dimension D_f is the parameter used to characterize the surface morphology. Furthermore, D_f should be, in principle, independent from the magnification values, going from macro or micro to nanoscale [42]. The power spectrum density (PSD) algorithm allows to estimate D_f for a surface. Each spectrum is the square of the surface roughness amplitude per spatial frequency k. The integral over all frequencies is the mean-square surface roughness within the measured bandwidth (σ^2). For example, a power spectrum has two distinct regions: the flat, low and very low frequency part resembling uncorrelated white noise and the sloped portion representing the correlated portion of the surface roughness. In the power spectral density showed in Figure 4, k values ranges from 5 μm^{-1} to 100 μm^{-1}; in this range only medium and high k frequencies are considered and a correlated behavior is evident. The PSD of an isotropic 2D fractal Brownian function varies as [14,15,38]

$$\mathrm{PSD} \propto k^{-B} \tag{1}$$

with $k = (x^2 + y^2)^{1/2}$ the radial frequency and $B \geq 0$ a characteristic exponent related to the fractal dimension [14,15,40,43]. So, B can be easily obtained plotting the PSD versus $1/k$ in an Arrhenius-type plot and fitting linearly the linear sloped portion of the spectrum. Appropriate values of k (from 30 to 90 μm^{-1} and from 10 to

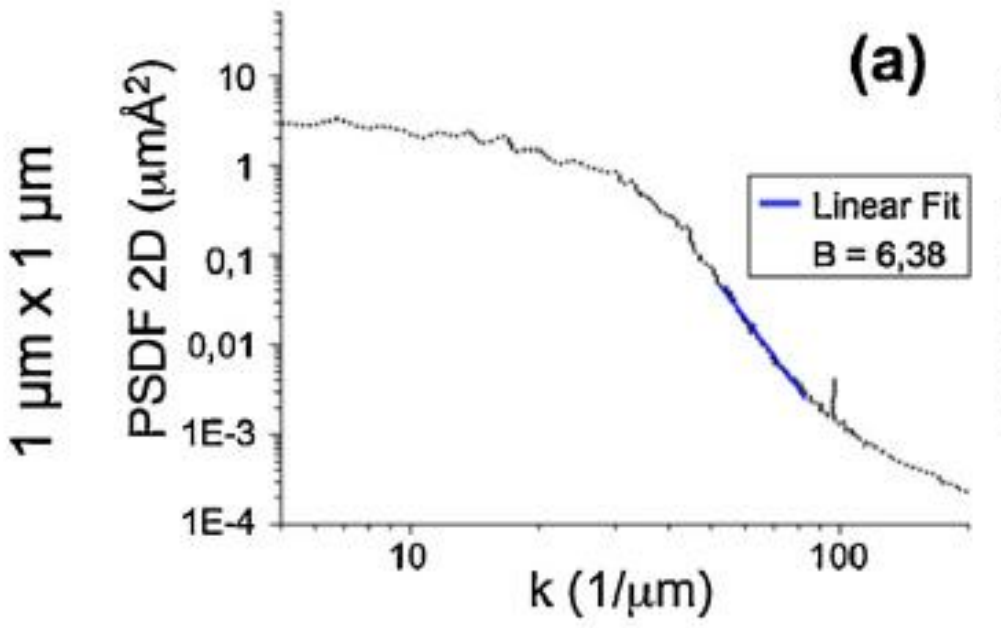

Now, the exponent B in Eq. (1) is related to the fractal dimension D_f by [14,15,43]

$$B = 8 - 2D_f. \quad (2)$$

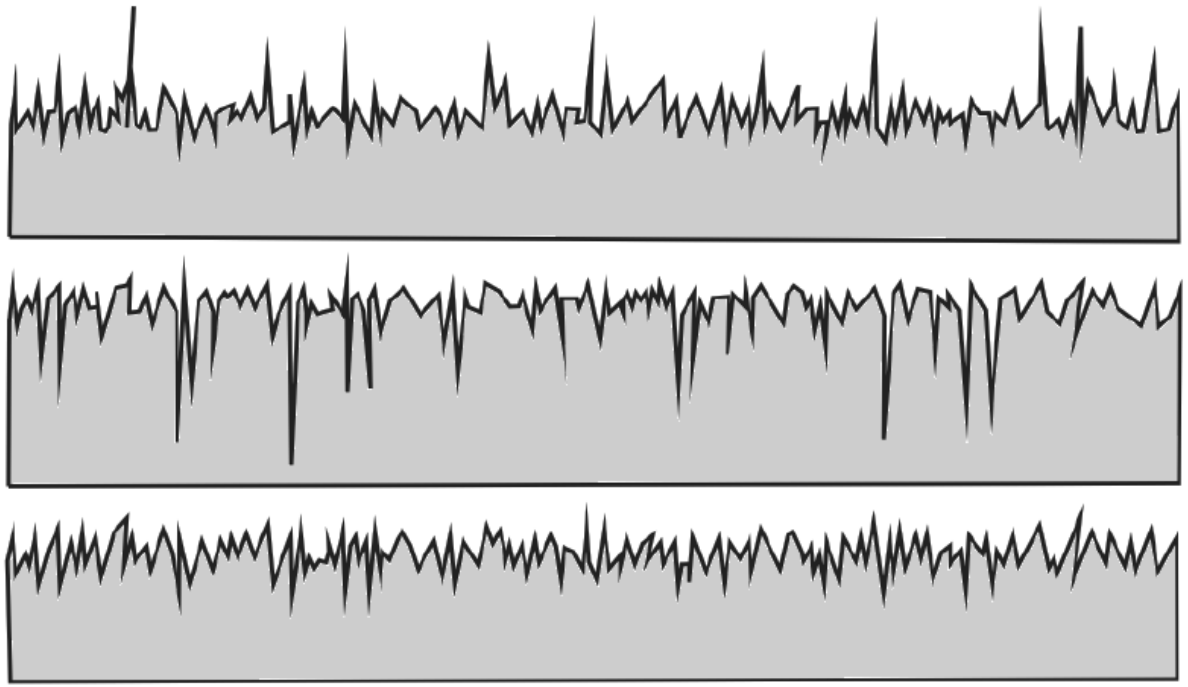

Fig. 13. Different profiles of surfaces, with the same roughness average (adapted from Predev, 2011).

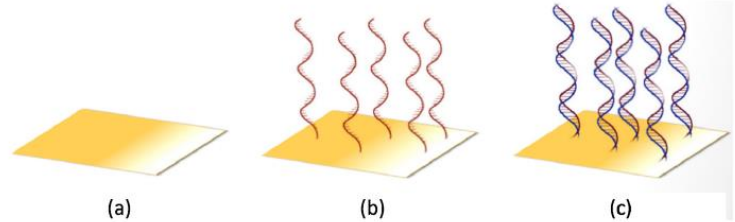

Figure 1. Schematic pictures of the analyzed samples: (a) bare Au surface, (b) Au surface after ssDNA immobilization, (c) Au surface after dsDNA hybridization.

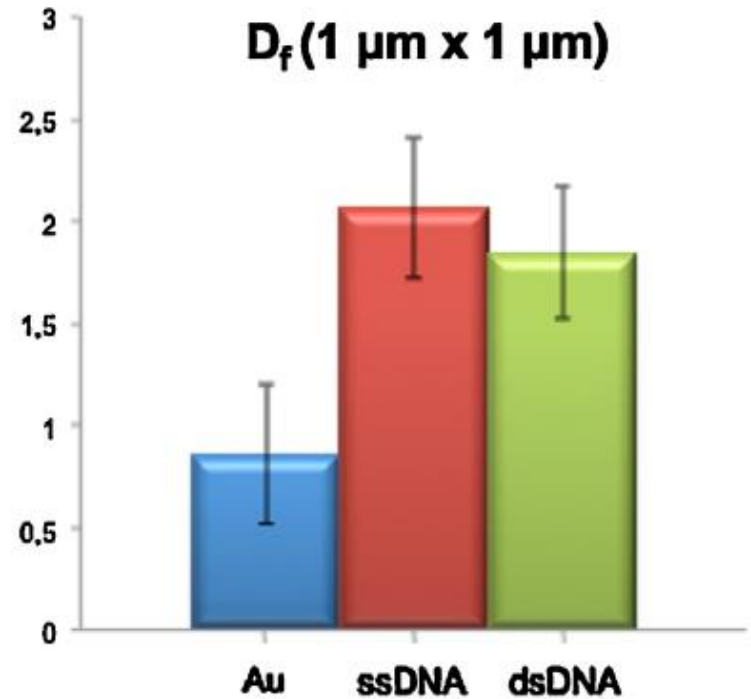

theory [40–42] we known that for a self-affine surface the fractal dimension D_f, should not be influenced by the magnification of the AFM images and it should be $2 \leq D_f \leq 3$ (2 for a Gaussian smooth surface). In spite of this, it is known that deposited metallic films on a surface growing by a Volmer–Weber mode (which is the case of Au on SiO_2 [44]) often present $D_f < 1.5$ [45]. A theory, developed by Fiorentini et al. [46], calculate a 1.2 value for film growing in a purely Volmer–Weber mode and it is verified, for example for deposited Al thin films by 3 μm × 3 μm AFM scans [45]. In particular deposition conditions, Au films have shown such a low D_f value: Gómez-Rodríguez et al. [47], used scanning tunneling microscopy to study the fractal dimension of vacuum-evaporated Au film. Their films grow by a Volmer–Weber mechanism originating nano-granular Au film composed of small clusters (<30 nm) corresponding to rounded shapes with Euclidean character. In this case, for such a film, they evaluated the fractal dimension $D_f = 1$. In other deposition conditions, they obtained a film composed by bigger and ramified clusters exhibiting fractal dimension $D_f = 1.72$. Similar results were obtained by Word et al. [48] they obtained a fractal dimension $D_f \approx 1.3$ for ramified Au film on surface.